A synthetic biology approach to probing nucleosome symmetry

Yuichi Ichikawa[1,*], Caitlin F. Connelly[2,*], Alon Appleboim[3,4,*], Hadas Jacobi[3,4], Nebiyu A. Abshiru[5], Hsin-Jung Chou[2], Yuanyuan Chen[1], Upasna Sharma[2], Yupeng Zheng[5], Paul M. Thomas[5], Hsiuyi V. Chen[2], Vineeta Bajaj[1], Neil L. Kelleher[5], Nir Friedman[3,4], Daniel N. Bolon[2], Oliver J. Rando[2]†, and Paul D. Kaufman,[1]†

[1]*Department of Molecular, Cell, and Cancer Biology, University of Massachusetts Medical School, Worcester, MA 01605, USA*

[2]*Department of Biochemistry and Molecular Pharmacology, University of Massachusetts Medical School, Worcester, MA 01605, USA*

[3]*School of Computer Science and Engineering, The Hebrew University, Jerusalem 91904, Israel*

[4]*Alexander Silberman Institute of Life Sciences, The Hebrew University, Jerusalem 91904, Israel*

[5]*National Resource for Translational and Developmental Proteomics, Northwestern University, Evanston, IL 60208 USA*

**Indicates authors contributing equally*

†To whom correspondence should be addressed.

E-mail: Oliver.Rando@umassmed.edu

E-mail: Paul.Kaufman1@umassmed.edu

ABSTRACT

The repeating subunit of chromatin, the nucleosome, includes two copies of each of the four core histones, and several recent studies have reported that asymmetrically-modified nucleosomes occur at regulatory elements in vivo. To probe the mechanisms by which histone modifications are read out, we designed an obligate pair of H3 heterodimers, termed H3X and H3Y, which we validated genetically and biochemically. Comparing the effects of asymmetric histone tail point mutants with those of symmetric double mutants revealed that a single methylated H3K36 per nucleosome was sufficient to silence cryptic transcription in vivo. We also demonstrate the utility of this system for analysis of histone modification crosstalk, using mass spectrometry to separately identify modifications on both H3 molecules within asymmetric nucleosomes. The ability to generate asymmetric nucleosomes in vivo provides a powerful tool to probe the mechanism by which H3 tails are read out by effector proteins in the cell.

INTRODUCTION

Packaging of eukaryotic genomes into chromatin has widespread consequences for genomic function, as nucleosomes generally impede the access of proteins to the underlying DNA (*1*). In addition, the histone proteins are subject to a huge variety of covalent modifications, which affect genomic function in ways ranging from direct alterations in the biophysical nature of the chromatin fiber to recruitment or activation of various regulatory proteins.

The histone octamer is comprised of two copies of each of the four histones H2A, H2B, H3, and H4, organized with two H2A/H2B dimers associated with a central core tetramer of histone H3 and H4 (*2*). The symmetry inherent to the histone octamer has long been appreciated, and it has been suggested that chromatin function may be regulated at the level of histone modification symmetry – that K4me3/K4me0 and K4me3/K4me3 nucleosomes might serve distinct functions in vivo, for example. Indeed, increasing evidence supports the existence of asymmetrically-modified nucleosomes in vivo. In mammals, immunopurification and mass spectrometry of nucleosomes

associated with H3K27me3 revealed a mixture of symmetrically-modified nucleosomes as well as asymmetric nucleosomes modified on only one H3 tail (*3*). More recent single molecule studies of H3K4me3/K27me3-marked “bivalent” nucleosomes reveal that the vast majority of these nucleosomes are asymmetrically modified, with each H3 tail bearing one of the two methylation marks, rather than both marks co-occurring on the same H3 molecule (*4*). In budding yeast, ChIP-Exo and chemical mapping studies identified a subset of nucleosomes that exhibit asymmetric contacts with the underlying genome (*5, 6*), suggested to reflect histone octamers associated with an asymmetrically-localized DNA bulge.

While evidence therefore increasingly supports the hypothesis that nucleosomes across the genome can be modified symmetrically or asymmetrically, at present it is largely unknown whether nucleosome symmetry affects genomic functions such as transcription. For instance, do any chromatin regulators bind specifically to singly-modified nucleosomes, or to doubly-modified nucleosomes? A handful of studies in vitro have suggested that chromatin regulators can distinguish singly-modified from doubly-modified nucleosomes. For instance, Li *et al* assembled and purified asymmetric nucleosomes lacking a single H3 tail in vitro, subsequently showing that the histone acetyltransferase Gcn5 exhibited cooperative binding to two histone tails (*7, 8*). Conversely, asymmetrically H3K4-methylated nucleosomes were, like unmodified nucleosomes, efficiently methylated at K27 by the PRC2 complex, whereas this methylation was inhibited by the presence of symmetric H3K4me3 marks (*3*). Although these in vitro studies generate hypotheses for how chromatin effectors might be affected by nucleosome symmetry in the cell, the inherent symmetry of the natural H3-H3 interface has made in vivo tests of these hypotheses impossible until now.

Here, we develop a novel system to enable analysis of the functional consequences of nucleosome symmetry in vivo. Using rational design, followed by in vivo optimization and selection, we developed a pair of H3 proteins – H3X and H3Y – that form heterodimers in vivo, yet cannot homodimerize. We validated this system genetically and biochemically in budding yeast, confirming that the vast majority of histone octamers in the cell contain a heterodimeric H3X/H3Y at their core. We used these heterodimers to probe several mechanistic aspects of nucleosome function in

vivo, finding that a single copy of H3K36 is sufficient for stress resistance, and to silence cryptic transcription, in vivo. In addition, we show that disruption of H3S10 affects H3K9 acetylation only on the same tail, demonstrating the utility of this approach for interrogating histone "crosstalk". This system thus represents a powerful approach to mechanistically probe the role of histone stoichiometry and symmetry in a variety of aspects of chromatin biology.

RESULTS

Design and validation of obligate heterodimers

The histone octamer is assembled around a central core tetramer of histone H3 and H4, assembled around a central H3-H3 homodimeric interface (*2*). In order to develop a system to analyze the role of nucleosome symmetry in chromatin regulation in vivo, we set out to design a pair of H3 molecules – "H3X" and "H3Y" – which cannot form X/X or Y/Y homodimers, but will efficiently form H3X/H3Y heterodimers (**Figure 1A**). We initially used protein design to develop six sets of H3 mutants that are predicted to have much higher affinity with a paired mutant protein than with wild-type H3. Each engineered variant had "bumps and holes" that are also predicted to reduce the potential for homodimerization. We focused our efforts on the hydrophobic cluster formed by amino acids L109, A110, L126, and L130 (**Figure 1B**) in the nucleosome structure (pdb 1kx3). At these positions, sequence and conformational space were enumerated using a rotamer description of side chain geometry and a molecular mechanics force-field (*9*) to generate a pairwise energy matrix. We used a previously described algorithm (*10*) to identify sequences that preferentially energetically partition as heterodimers.

We then carried out genetic tests of six initial designs in vivo, reasoning that budding yeast carrying both H3X and H3Y should be viable, but yeast carrying H3X alone or H3Y alone would be inviable due to the failure of these H3 molecules to homodimerize. In our initial tests, one of the original six designs (H3X = L126V, L130V; H3Y= L109I, A110W, L130I) exhibited most of the expected growth behaviors. However, although yeast carrying H3Y alone exhibited no growth even after 21 days of

culture (**Figure 1C** and not shown), H3X-only strains did grow even in the absence of H3Y, albeit poorly – colonies were only observed after nine or more days of growth of these strains (**Figure 1 – Figure Supplement 1A**), in contrast to the abundant colonies observed for H3X/H3Y strains after just two or three days. As homodimerization of H3X even at low levels could complicate interpretation of this system, we carried out a round of in vivo selection to optimize the H3X interface (**Figure 1 – Figure Supplement 1B-C**). We randomized each of the H3/H3 interface residues on the backbone of the initial H3X gene, generating libraries of yeast strains bearing these mutant "H3X*" molecules paired with our previously-selected H3Y design. Strains that grew robustly with H3X*/H3Y pairs were then re-tested for growth in the absence of the H3Y. In this manner, we identified four final versions of H3X (named 126A, 130A, 130T, and 130Q for the additional substitutions on the original H3X backbone) that reproducibly conferred robust growth in the presence of H3Y but were completely inviable in its absence (**Figure 1D-E**). We obtained multiple isolates encoding each of these amino acid substitutions (13, 5, 5, and 5, respectively), suggesting that we had adequately surveyed the possible codons. Consistent with our observation that these residues are sensitive points for H3/H3 dimeric interactions, L126A and L130A mutations cause lethality when present on symmetric H3 molecules (*11*).

Although these genetic tests demonstrate that H3X or H3Y alone do not homodimerize efficiently enough to support growth, the possibility remains that in the context of cells expressing both H3X and H3Y there could nonetheless exist a substantial fraction of inappropriate homodimeric interactions, which would complicate interpretation of downstream results. To quantitatively determine the extent of X/X or Y/Y homodimerization in vivo, a biotin-tagged (*12*) H3X or Y variant was coexpressed in combination with two other H3s: the same variant with a different epitope tag, and the designed partner (**Figure 2**). To analyze H3-H3 interactions within individual nucleosomes and avoid contamination from adjacent nucleosomes (as could arise from undigested dinucleosomes), we treated extracts from these cells with dimethyl suberimidate (DMS), a crosslinking agent that produces well-characterized crosslinks within histone octamers (*13, 14*). Crosslinked samples were then digested with micrococcal nuclease to generate a soluble population of mononucleosomes. This was

followed by biotin-based affinity purification in the presence of high salt (2M NaCl) to remove DNA, leaving only crosslinked protein complexes that were subsequently analyzed by Western blotting. Using this assay, we analyzed the extent of homodimerization of a lead H3X candidate using strains expressing Biotin-H3X, V5-H3X, and Myc-H3Y (**Figure 2A-C**). After streptavidin purification of biotin-H3X from DMS-crosslinked yeast, the species migrating at 31kD (red arrow, **Figure 2B**) is comprised of the captured biotin-H3X crosslinked to the other H3 from the same nucleosome. Myc-H3Y molecules were abundantly detected in the crosslinked 31kD species (**Figure 2B, Figure 2 – Figure Supplement 1**), consistent with the expected heterodimerization with H3X. In contrast, barely detectable levels of V5-H3X were observed in the bound 31kD species (**Figure 2B**, quantitated in **Figure 2C**). As similar results were obtained with the 126A and 126V versions of the H3X protein, we arbitrarily chose the 126A variant to serve as the primary H3X used for the studies below.

Taken together, our genetic and biochemical analyses validate our designed obligate heterodimers, indicating that the great majority (at least 96% – **Figure 2C**) if not all of the nucleosomes in vivo are indeed heterodimeric. We have therefore established a unique system for manipulation of nucleosomal symmetry in vivo.

Genetic analysis of interactions between histone tail mutations

The ability to generate asymmetric nucleosomes in vivo enabled us to quantitatively characterize interactions between mutations on the two histone tails using genetic epistasis. To this end, we generated “trios” of histone point mutants – asymmetric single mutations H3Xwt/H3Y**mut** and H3X**mut**/H3Ywt, and the double mutation H3X**mut**/H3Y**mut**. Any effects of the mutant X/Y interface on chromatin regulation and cellular function are internally controlled for by comparing all yeast carrying single or double histone mutations to the “pseudo-wild type” strain (H3Xwt/H3Ywt).

To broadly survey the landscape of inter-tail epistasis between histone mutations, we generated a set of 12 mutant trios, focusing on relatively well-characterized sites of post-translational covalent modifications. As mutant effects on organismal phenotypes are often context-dependent – stress conditions can provide a sensitized environment for detection of chromatin-related phenotypes (*15*) – we first

assayed the relative fitness of these strains in both low (0.2 M) and high (0.8 M) KCl-containing media (**Figure 3A**). As expected, growth rates for strains carrying a single mutation on H3X were generally well-correlated with those for H3Y mutants, although a small subset of mutations exhibited different behavior on different H3 backbones (see, eg, H3K37Q in 0.8M KCl).

Consistent with the often-subtle phenotypes resulting from histone point mutations, the majority of mutations examined conferred no significant growth defects under either growth condition, or subtle growth effects such as the enhanced growth observed in all three H3K18Q strains growing in high salt. In contrast, we noted significantly diminished growth, particularly in high salt, for yeast carrying double H3K14R or H3K36Q mutations (**Figure 3B, Figure 3 – Figure Supplement 1**). Interestingly, the behaviors of the corresponding asymmetric single mutants were distinct: for H3K14R, single mutants already exhibited a partial growth defect that was exacerbated in the double mutant, while for H3K36Q the single mutant strains had no measurable deficit compared to the pseudo-wild type. These growth phenotypes correspond roughly to additive and recessive epistasis, respectively. Importantly, the stress sensitivity observed for these mutants was not specific to osmotic stress, as these mutants were also temperature-sensitive – symmetric double mutants exhibited reduced growth at 34 C, while the asymmetric mutants exhibited similar or slightly reduced growth compared to the pseudo-wild type under these conditions (**Figure 3C, Figure 3 – Figure Supplement 2**).

A single H3K36 suffices to silence cryptic internal promoters

We conclude from these data that a single copy of H3K36 per nucleosome is sufficient to support growth under stress conditions. What is the mechanistic basis for this function? In principle, mutation of this lysine could 1) affect biophysical properties of the nucleosome by eliminating a positive charge, 2) disrupt a binding site for regulatory protein that binds to the unmodified tail, or 3) disrupt (or mimic) a modification-dependent regulatory event. H3K36 is methylated by Set2 (*16*), with the resulting modified residues serving to activate the RPD3S histone deacetylase complex via binding of the Eaf3 chromodomain-containing subunit (*17-20*). As the major biological

role served by H3K36 methylation is silencing of cryptic internal promoters via activation of the RPD3S complex (*17*), and given that RPD3S can bind to nucleosomes with a single H3K36me3 modification (*21*), we sought to test whether a single methylated H3K36 per nucleosome would be sufficient to support robust silencing of such cryptic transcripts in vivo.

We first explored this idea with genetic tests, comparing the growth phenotypes of a P38V mutant series to K36Q mutants. The P38V mutants enable di- and tri-methylation of H3K36 to be distinguished – the wild-type proline residue at this position undergoes regulated isomerization, and P38V mutations that eliminate the possibility of proline isomerization block trimethylation (*22*) but not dimethylation (*23*) of the nearby K36 residue. Importantly, cells expressing only H3P38V display none of the cryptic transcription phenotypes observed in *set2*, *eaf3*, or H3K36Q mutants ((*23*) and see below), indicating that H3K36me2 is sufficient for the proper activation of the Rpd3S complex with regards to repression of cryptic transcription. Consistent with this, we find that double P38V mutations, on either a wild-type H3 backbone or in the context of the XY system, did not cause the temperature sensitivity observed in K36Q mutant cells (**Figure 3D, Figure 3 – Figure Supplement 2**). We therefore hypothesized that a single H3 N-terminal tail bearing K36 di- or trimethylation is sufficient to repress cryptic transcription.

To determine whether the single methylated K36 must be trimethylated or whether dimethylation is sufficient, we generated strains carrying the K36Q and P38V mutations in a trans conformation, that is, on opposite H3 N-termini (**Figure 3E**). These strains have one H3 tail (K36Q) that lacks K36 methylation entirely, and one tail (P38V) with a dimethylated K36 residue. We made strains with both possible configurations: H3XK36Q + H3YP38V and H3XP38V + H3YK36Q. Notably, neither of these K36Q/P38V trans strains are sensitive to growth at 34C. Thus, they phenotypically resemble the P38V double mutants and the single K36Q mutants, rather than the temperature-sensitive K36Q double mutants. These data indicate that a single K36me2 is sufficient to promote stress tolerance in budding yeast.

To determine whether the growth data reflect underlying defects in control of cryptic transcription, we carried out Northern blots against a canonical target of this

pathway – *STE11* – which is host to a well-characterized cryptic promoter that is silenced in a K36- and RPD3S-dependent manner (*17, 18l, 19*). First, we confirmed the expected increase in cryptic transcription in *eaf3*Δ mutants, and in yeast carrying symmetric H3K36Q mutations on the wild-type H3 backbone (**Figures 4A-B**, lanes 1-4). H3K36me2 was sufficient to silence the *STE11* cryptic promoter, as H3P38V mutants (which lack H3K36me3 but exhibit normal H3K36me2 levels) did not cause significantly increased cryptic transcription (lane 5).

Turning next to the question of whether one H3K36 is sufficient for silencing, we analyzed *STE11* RNAs in single and double H3K36Q mutants in the H3X/Y backbone (**Figure 4**, lanes 6-9). Consistent with the growth phenotypes observed in **Figure 3**, we find that the pseudo-wildtype H3X/Y cells and the cells with a single K36Q mutated tail display similar, low levels of cryptic transcripts (lanes 6-8). In contrast, the cells with two K36Q mutated tails display greatly elevated cryptic transcript levels. As expected, neither single nor double P38V mutant tails affected cryptic transcription in our strain background (lanes 14-16). Similar results were obtained for another well-studied model for cryptic transcription, the *FLO8* locus (*24*), confirming the generality of this finding (**Figure 4 – Figure Supplement 1**). We conclude that a single K36-methylated H3 tail per nucleosome is sufficient to restrain cryptic transcription in vivo.

Interrogating histone crosstalk in cis and trans

In addition to our ability to uncover effects of asymmetric mutant nucleosomes on transcriptional regulation, our system also provides a unique opportunity to determine whether histone “crosstalk” – the ability of one histone modification to alter the level of another modification via effects on modifying enzyme recruitment or activity (*25*) – occurs in cis (on the same histone), or in trans. We generated biotin-tagged H3 molecules either carrying a point mutation of interest in cis, or carrying an otherwise wild-type sequence on the biotin-tagged H3, paired with a point mutation in trans. Biotin-tagged H3 molecules were then purified under stringent, partially denaturing conditions to facilitate the separation of H3X and H3Y, and the biotin-tagged H3 was subject to mass spectrometry to identify histone modifications present. Analysis of peptides derived from the engineered H3X/H3Y interface confirmed our ability to efficiently purify

the biotin-tagged H3 molecule away from the untagged H3 molecule from each nucleosome, with >93% purity observed for informative peptides analyzed (**Figure 5A**).

As cases of histone crosstalk that occur between different histones (e.g. effects of H2B ubiquitylation on H3 methylation levels) cannot be interrogated using our system, we focused on H3S10, whose phosphorylation affects histone H3 lysine acetylation (*26*). Consistent with prior reports, we found that the fraction of H3 molecules acetylated at K9 was lower in yeast strains carrying H3S10A symmetrically, either on a wild-type histone backbone or in the H3X/H3Y system. This decrease was observed by mass spec, and confirmed by quantitative Western blot (**Figures 5B and C,** left panel). Turning next to analysis of asymmetric mutant nucleosomes, mass spectrometric analyses showed that H3K9 acetylation levels were significantly decreased on the same histone tail carrying the S10A mutation, but were not affected by the presence of H3S10A in trans (**Figure 5B**). Western blotting for H3K9ac in yeast strains where an epitope tag allows H3X and H3Y isoforms to be separated by gel electrophoresis confirmed our mass spec-based analysis of histone acetylation, with H3S10A affecting adjacent H3K9 acetylation on the same tail, but having no effect on modification of a paired wild-type H3 tail (**Figures 5C-F**).

DISCUSSION

Here, we demonstrate a novel system enabling genetically-encoded symmetry breaking for the histone octamer. Using protein engineering and directed evolution, we have designed and validated a pair of H3 variants – H3X and H3Y – that efficiently heterodimerize with one another in vivo, but which form extremely low levels (<4%) of homodimers. The ability to generate nucleosomes bearing either single mutations or symmetric double mutations to key regulatory residues will allow detailed mechanistic analyses of the roles for histone modifications in various aspects of chromosome biology. As with all studies based on expression of mutant histones, the mutant nucleosomes will be located throughout the yeast genome. Nonetheless, such studies have provided great insights into chromatin function over decades of study (*11, 27*), distinguishing between genes whose expression requires a given histone residue and

those genes that are unaffected despite the loss of the residue (and its modification, if present).

Here, we demonstrate two of many potential uses of this system, interrogating the role for H3K36 in control of cryptic transcription, and investigating “crosstalk” between histone modifications.

Interpreting epistasis between the histone tails

To genetically interrogate interactions between the histone tails, we analyzed phenotypes in yeast strains carrying one of four nucleosomes: H3Xwt/H3Ywt – “pseudo-wild-type” – and H3X**mut**/H3Ywt, H3Xwt/H3Y**mut**, and H3X**mut**/H3Y**mut**. In principle, we could expect to see a variety of classes of interactions between the mutants, including transgressive epistasis (not observed in this study), and a range from dominant epistasis, in which the single mutants exhibit the same phenotype observed in the double mutant, to recessive epistasis, in which a given phenotype is only observed in the double. For quantitative traits, these correspond to aggravating and alleviating epistasis, respectively (*28*).

Measured in the context of obligate heterodimers, such genetic interactions can provide insights into the mechanistic basis for readout of histone modifications. As a simple example, a protein that binds cooperatively to both tails of a given nucleosome should give rise to dominant epistasis between the histone mutations that affect its binding, as loss of a single residue abrogates the cooperative binding. Conversely, if each histone tail recruits a binding protein independently of one another, then loss of a single tail could have a range of quantitative effects on local gene expression depending on whether or not the binder is typically recruited in excess for some function. Downstream of initial binding interactions, many readouts of histone modification function, such as mRNA abundance, are several mechanistic steps removed from direct binding, and thus more complex models can readily be envisioned that would exhibit a range of distinct epistasis behaviors depending on the input/output relationships for the various intervening steps.

Here, we surveyed intra-tail epistasis for 12 sets of H3 point mutants, simply using growth rate as a phenotype. Even with this coarse resolution, we identified a inter-

tail interactions including dominant epistasis (for the enhanced low-salt growth seen in H3K18Q mutants, for example) to relatively unusual cases of recessive epistasis (for H3K36Q effects on growth in stress conditions). For followup studies we focused on H3K36Q, given that recessive epistasis makes more concrete mechanistic predictions, and given the well-understood role for modification of this residue in gene regulation.

A single H3K36me2 per nucleosome is sufficient for stress resistance and repression of cryptic transcripts

Although H3K36 is potentially subject to multiple distinct modification pathways – H3K36 is acetylated at a small fraction of nucleosomes (*29*), for example – the majority of phenotypes of H3K36 mutants result from loss of Set2-dependent methylation of this residue (*17, 18l, 19*). Our system thus allows us to ask, essentially, whether a single RPD3S binding site per nucleosome is sufficient to repress cryptic internal promoters.

Several lines of evidence demonstrate that a single H3K36me2 is sufficient for RPD3S silencing at the majority of cryptic promoters. First, we find that H3K36Q significantly affects growth rate – particularly under stress conditions – only when present in both H3 copies per nucleosome. Next, consistent with a primary function of H3K36 modification being to repress cryptic intragenic promoters, we show that a single wild-type K36 is sufficient to prevent transcription at such promoters. Third, extending prior studies, we find that growth rate and cryptic promoter silencing are both unaffected by double P38V mutants. P38V inhibits trimethylation but not dimethylation of K36 residues (*23*), and nucleosomes with two H3P38V tails are sufficient to prevent cryptic transcription either in natural, symmetric nucleosomes (*23*) or in our asymmetric nucleosomes (**Figure 4**, lane 16). Finally, the K36Q/P38V trans strains indicate that a single dimethylated K36 residue is sufficient to prevent stress sensitivity (**Figure 3E**). Together, these data indicate that a single K36-dimethylated H3 tail per nucleosome is sufficient to prevent cryptic transcription, and to promote stress resistance.

Notably, the RPD3S complex appears to be particularly well-suited to carrying out its regulatory functions even on chromatin that is less than fully methylated at H3K36. In vitro experiments show that RPD3S is able to bind to nucleosomal templates containing asymmetric H3K36me3 modifications (*21*). Further, although RPD3S binds

with higher affinity to dinucleosomes than monosomes, it binds with high affinity to templates with a dimethylated nucleosome adjacent to a fully unmethylated one. These data suggest that the K36me3/RPD3S system would be buffered against transient reductions in H3K36me3 density, for example during DNA repair or replication-mediated loss of modified histones. Our data extend these observations to indicate that the enzyme can function effectively in vivo even if it can only engage a single H3K36me2 or me3 per nucleosome.

H3S10 mutants affect H3K9 acetylation in cis

As another demonstration of the utility of the H3X/H3Y system, we carried out mass spec analysis of a histone "crosstalk" pathway. Here, we take advantage of biotin-based purification to stringently separate a biotin-tagged H3X from an untagged H3Y (and vice versa) prior to mass spec analysis. This method allows probing of histone crosstalk pathways, in which one modification affects a second modification site. We show that H3S10A mutations decrease acetylation at the neighboring K9 residue, but only on the molecule in cis. This dependency relationship is distinct from "phospho/methyl switch" interactions, in which phosphorylation of histone residues such as H3S3, 10 or 28 (reviewed in (*30*)) affects affinity of "reader" proteins for neighboring methylated lysines. That is, our data indicate that lack of phosphorylation caused by S10A mutations inhibits neighboring K9 acetylation, and does so only in cis, presumably reflecting poor binding of the mutant peptide substrate to the acetyltransferase active site (*26*). This example provides a clear example of how asymmetric nucleosomes can be used for detecting modification dependency relationships.

Perspective

Together, our data demonstrate the utility of in vivo analysis of asymmetric nucleosome as a mechanistic probe for histone modification function. Given the extreme conservation of histone protein sequences, we anticipate that this system should be portable into other species in which canonical histone genetics are feasible (*31*), and

could also be applied in any species to low copy number histone H3 variants such as H3.3 or CENPA.

ACKNOWLEDGEMENTS

We thank members of the Rando and Kaufman labs for discussions and critical reading of the manuscript. This work was supported by NIH grant R01GM100164 (OJR and PDK), ERC Grant 340712 (NF), and the ISF I-Core on Chromatin and RNA in Gene Regulation (NF). Proteomics experiments were supported by NIH grants P30CA060553 and P41GM108569. AA is grateful to the Azrieli foundation for the award of an Azrieli Fellowship.

MATERIALS AND METHODS

Plasmid Constructions and mutagenesis. C-terminal mutations of *HHT2*, one of the yeast genes encoding histone H3, were generated according to QuickChange Site-Directed Mutagenesis protocol (Stratagene). Plasmids containing Myc- or Flag-tagged *HHT2* were described previously (*32*). The insertion of the V5 or biotin acceptor tags at the 5' end of *HHT2* was generated by PCR. The DNA fragment containing the *E. coli BirA* gene (encoding biotin-protein ligase) (*12*) was cloned into a *HIS3*-marked integration vector downstream of the yeast *GPD* promoter and upstream of *PGK* terminator, and integrated into the *his3* locus of strain PKY4171.

Yeast strains and growth. Yeast growth and plasmid transformation of yeast cells were done according to standard yeast protocols. Low-copy plasmids containing mutated histone genes were introduced by LiOAc transformation, and then 5-FOA was used as a counterselecting agent to select against the *URA3* plasmid containing the wild-type *HHT1-HHF1* genes.

All yeast strains (listed in **Table S1**) were derived from histone H3/H4 “shuffle” strain MSY421 from M. Smith and C.D. Allis (*33*), which has both chromosomal H3/H4-encoding loci deleted.

Genetic screens for asymmetric mutants were carried out in:
PKY4171
MAT**a**; Δ(*hht-hhf1*); Δ(*hht2-hhf2*); *leu2-3,112*; *ura3-62*; *trp1*; *his3*; *bar1::hisG*
+ p(*HHT1-HHF1*, *URA3*, CEN)

DMS crosslinking studies:
PKY4171 derivatives with (*HHT1-HHF1, URA3*) plasmid replaced with:

PKY4625
+ P22 (Myc-H3Y = Myc-hht2(L109I, A110W, L130I), HHF2, LEU2)
+ P67 (bio-H3X-126A = biotin-hht2(L126A, L130V), HHF2, TRP1)
+ P72 (V5-H3X-126A = V5-hht2(L126A, L130V), HHF2, URA3)

PKY4626
+ P22 (Myc-H3Y = Myc-hht2(L109I, A110W, L130I), HHF2, LEU2)
+ P71 (bio-H3X-130A = biotin-hht2(L126V, L130A), HHF2, TRP1)
+ P73 (V5-H3X-130A = V5-hht2(L126V, L130A), HHF2, URA3)

PKY4694
+ P54 (biotin-H3Y = biotin-hht2(L109I, A110W, L130I), HHF2, LEU2)
+ P72 (V5-126A = V5-hht2(L126A, L130V), HHF2, URA3)
+ P35 (Myc-H3Y = Myc-hht2(L109I, A110W, L130I), HHF2, TRP1)

PKY4695
+ P54 (biotin-H3Y = biotin-hht2(L109I, A110W, L130I), HHF2, LEU2)
+ P73 (V5-130A = V5-hht2(L126V, L130A), HHF2, URA3)
+ P35 (Myc-H3Y = Myc-hht2(L109I, A110W, L130I), HHF2, TRP1)

Mass spectrometry samples were grown in derivatives of
PKY4574 = PKY4171 with P65 (BirA::HIS3 integration plasmid) inserted.

Directed evolution of improved H3X alleles. Plasmid P46 (*hht2*-(L126V, L130V), *HHF2*, *TRP1*) was used as the template to generate four PCR-generated libraries, each with randomized nucleotides at one of four H3 codons (109, 110, 126, 130). The full length PCR product was gel purified, self-ligated with T4 DNA ligase and transformed into competent E. coli Top10F' cells. 1 ml LB was added after heat shock transformation and the cells recovered for 1.5 h at 37°C. 100 µl cells were plated to check the colony number, and the rest of the transformation was put into culture tube with another 2 ml LB and antibiotic to grow O/N before plasmid DNA miniprep (Zymo). The randomization of the desired codon in the four libraries of *hht2* was confirmed by sequencing (**Figure 1 – Figure Supplement 1B**).

The four libraries were each transformed separately into yeast strain PKY4171, which carries the plasmid-borne wild-type H3 (*URA3*). 153 transformants were picked for each library and patched onto both SD-Trp-Ura and FOA plates at the same time. A subset of isolates were found inviable after incubation at 30°C for 10 days on FOA, indicating inability to grow the absence of wild type H3. These isolates were therefore chosen for the second step. For each library separately, cells from each FOA-sensitive isolate were pooled into 25 ml of SD media, grown to an A600 of ~0.5 and transformed with plasmid P44 (H3Y, H4, *LEU2*) and plated on SD-Trp-Leu. These transformants were then replica-plated onto FOA media. Plasmids from resulting FOA-resistant colonies were analyzed by colony PCR and sequencing. Candidate plasmids were retested by retransformation into PKY4171 with or without P44. The plasmids that conferred robust growth on FOA media in the presence of P44 and no detectable growth in its absence encoded the *hht2* variants termed 126A (carrying mutations 126A, 130V), 130A (126V, 130A), 130T (126V, 130T), 130Q (126V, 130Q).

Differences between "pseudo-wild type" H3X/H3Y yeast and BY4741: plate growth assays

As asymmetric nucleosomes cannot be made on a wild-type H3 backbone, all experiments by necessity involve comparisons to pseudo-wild type yeast carrying the H3X/H3Y pair. Pseudo-wild type yeast are viable and grow well under standard laboratory conditions (**Figure 3**), but are temperature-sensitive and grow extremely poorly at 37°C. For this reason, temperature sensitivity in this system is assayed at 34°C (**Figure 3C-E, Figure 3 – Figure Supplement 2**). For this assay, strains were grown overnight in 2 ml YPD medium at 30°C. Five-fold dilutions (start from OD_{600}=0.6) were spotted on YPD-agar plates. Plates were incubated at indicated temperature for 3-4 days.

Dimethyl suberimidate-crosslinked nucleosomes.

100 ml cell cultures were grown in synthetic dextrose media to maintain selection for the three histone-encoding plasmids, with 250 nM biotin added to favor biotinylation of the tagged H3. Cells were harvested in early log phase (A600 ~0.25), pelleted and transferred to 1.5 ml O-ring microcentrifuge tubes (Fisher #02-707-353). Cells were washed three times with 1 ml extraction (E) buffer (20 mM Na borate, pH 9.0, 0.35 M NaCl, 2 mM EDTA, plus 1 mM PMSF added freshly). Cells were resuspended in 900 μl E buffer, and 0.5 ml glass beads (0.5 mm, Biospec) were added to each tube. Cell walls were mechanically broken with three one-minute pulses in a Biospec beadbeater, with five-minute incubations on ice between pulses. The tube bottoms were punctured with a flame-heated 26 gauge needle, placed into a 12 x 75 mm plastic tube and centrifuged for 2 min at 1500 rpm in a tabletop clinical centrifuge at 4°C. The liquid extracts were resuspended and transferred to 1.5 ml microfuge tubes. 1/10 volume freshly dissolved 11 mg/ml dimethyl suberimidate (Pierce) in E buffer was added, and samples were incubated with rotation at room temperature 90 minutes. For time point aliquots to be analyzed directly on gels, proteins were precipitated by addition of 1/10 volume 100% TCA. For material to be MNase-digested and immunoprecipitated, the crosslinker was quenched by addition of 50 mM Tris-Cl, pH 7.5 and further rotation for 15 min. 10 mM MgCl2 and 1 mM CaCl2 were added and tubes were equilibrated at 37°C for 5 minutes. 20 μl MNase (Worthington, 20 U/μl in 10 mM Tris-Cl pH7.4) were added, tubes were inverted five times and incubated at 37°C, 20 min. Digestion was stopped by moving

tubes to 4°C, adding 40 μl 0.25 M EDTA/EGTA and inversion to mix. Material was centrifuged at 8000 x g for 1 min, 4°C, and pre-cleared by incubation with CL2B-sepharose beads for 30 min 4°C and centrifugation at 8000 x g for 1 min, 4°C. The supernatant was the input for the pulldown assays. 30 μl of a 50% slurry of streptavidin-agarose beads was added to each tube, followed by rotation for 2 hours at 4°C. Samples were then centrifuged at 8000 x g for 1 min, 4°C and the beads were washed three times w/ 1 ml TE + 2 M NaCl + 0.2% Tween20, rotating at 4°C for 5 min each time. After the last wash all supernatant was removed and beads were resuspended in protein gel sample buffer. Proteins were separated on 17% SDS-PAGE gels and analyzed by immunoblotting; the 31kD H3-H3 crosslinked species was quantified on a BioRad Chemidoc system.

Mass spectrometric analysis of biotinylated H3 from asymmetric nucleosomes. 1000 ml cultures were grown in YPD + 250 nM biotin at 30°C to mid-late log phase (A600 = 0.4-0.7). Then, sodium azide and phenylmethylsulfonyl fluoride were added to the medium at final concentrations of 0.1% and 5 mM, respectively. Cells were pelleted and collected into two to four O-ring tubes as above, and washed twice with buffer TG (0.1 M Tris-Cl, pH 8.0, 20% glycerol) + protease/deacetylase/phosphatase inhibitors: 1 mM PMSF, 0.5 μg/ml leupeptin, 0.7 μg/ml pepstatin, 1.0 μg/ml E64, 1.0 μg/ml aprotinin, 1 mM benzamidine) + 20 mM Na butyrate, 2 mM nicotinamide, 1 mM EDTA, 1 mM Na3VO4. Tubes were frozen in liquid nitrogen and stored at -80C. All subsequent steps were on ice or at 4°C.

Each tube of frozen cells was resuspended in 900 μl TG buffer with the inhibitors described above, plus 0.5 ml glass beads (0.5 mm, Biospec). Cell walls were broken by bead beating, and beads were removed as described above. Liquid extracts were transferred to 1.5 ml eppendorf tubes, and centrifuged 7K rpm, 5 min (4.5K x g). The cytosolic supernatant was removed and the pellet was resuspended in 1 ml Buffer L (50 mM Hepes-KOH pH 7.5, 140 mM NaCl, 1 mM EDTA, 1% Triton X-100, 0.1% sodium deoxycholate) + inhibitors as described above. Chromatin was sheared in a Bioruptor (Diagenode) for 30 min (2 x 15 minute rounds of 30'' on/30" off on "High" power; samples were chilled on ice 10 minutes between rounds). Extracts were transferred to

microfuge tubes, centrifuged at 6K rpm (= 3.3K x g) for 10 min. The supernatant was the input for the pulldown assays. 30 μl of a 50% slurry streptavidin-agarose beads was added to each tube, followed by rotation for 2 hours at 4°C. (Beads were pre-equilibrated and blocked in Buffer L + inhibitors + 10 μg insulin per sample.) Samples were centrifuged at 8000 x g for 1 min, and the beads were washed three times with 1 ml TE + 2 M NaCl + 2 M urea, rotating at 4°C for 5 min each time. To remove salt for mass spectrometry, beads were washed three times with water, snap-frozen and stored at -80°C.

On-bead histone propionylation and tryptic digestion. Biotin-tagged histone H3 bound to streptavidin beads were washed twice with 300μl of 100mM ammonium bicarbonate. For in vitro propionylation of histone H3, 300μl of a 3:1 isopropanol:propionic anhydride mixture was added followed by ammonium hydroxide to adjust pH to ~8. The beads were incubated at 51°C for 20 min. Beads were then collected by centrifugation at 1000 rpm for 60 s and washed with ammonium bicarbonate before a second round of propionic anhydride treatment. The washed beads were resuspended in 50mM ammonium bicarbonate and incubated with 2μg of Promega sequencing grade trypsin overnight at 37^{0}C. The digest was then derivatized with propionic anhydride using the same protocol as described above. Histone peptides were extracted from the beads with 200 μl of 50% acetonitrile in water. Peptides were completely dried in a SpeedVac concentrator and then resuspended in 0.1% triflouroacetic acid for MS analysis.

Liquid chromatography single reaction monitoring mass spectrometry (LC-SRM-MS). Histone peptides were injected in triplicate onto a TSQ Quantum mass spectrometer (ThermoFisher Scientific) directly linked to a Dionex nano-LC system. Peptides were first loaded onto a trapping column (3 cm × 150 μm) and then separated with an analytical capillary column (10 cm × 75 μm). Both were packed with ProntoSIL C18-AQ, 3μm, 200Å resin (New Objective). The chromatography gradient was achieved by increasing percentage of buffer B from 0 to 35% at a flow rate of 0.30 μl/min over 45 min. Solvent A: 0.1% formic acid in water, and B: 0.1% formic acid in 95% acetonitrile.

The peptides were then introduced into the MS by electrospray from an emitter with 10 µm tip (New Objective) as they were eluted from analytical column. The instrument settings were as follows: collision gas pressure of 1.5 mTorr; Q1 peak width of 0.7 (FWHM); cycle time of 3 s; skimmer offset of 10 V; electrospray voltage of 2.5 kV. Targeted analysis of unmodified and various modified histone peptides were performed.

Raw MS files were imported and analyzed in Skyline with Savitzky-Golay smoothing (*34*). All Skyline peak area assignments were manually confirmed. Total peak areas normalized to a non-modified H3 peptide were used to plot bar graphs representing relative proportions of distinct histone modifications. The relative abundances were determined from the mean of three technical replicates with error bars showing standard deviation.

Northern Blot Analysis

Cells were grown in YPD medium to mid-exponential phase (OD_{600} = 0.4 to 0.7), and collected by filtration. RNA was prepared by a hot phenol method (*35*). Northern blot analysis was performed as described previously (*36*) with following modifications: *STE11* and *FLO8* PCR fragments (*37*) were used as probes that were labeled with alkaline phosphatase using Amersham AlkPhos Direct Labeling and Detection Systems (GE healthcare). Blots were exposed to HyBlot CL Autoradiography Film (Denville Scientific). Signal intensity was quantified by using ImageJ.

Primers for Northern probe (*37*)

o-STE11-11: GAA GGA GTT ACA TCA TGA GAA CAT TGT TAC

o-STE11-12: GTG TGC ATC CAG CCA TGG ATG CTG CAG CAA

o-FLO8-13: GAC GCT CAG AAG CAA AGA AGT TCT AAG GTA

o-FLO8-14: CTC AAC ACG TGA CTT CAG CCT TCC CAA TTA

FIGURE LEGENDS

Figure 1: Design and testing of asymmetric nucleosomes.

A) Schematic of asymmetric histone H3 design. Left: Wild-type H3/H4 tetramers are symmetrical, with H3-H3 interactions serving as the dimerization interface. The H3 N-terminus, site of many modifiable residues, is indicated protruding from the globular domain. Right: Obligate heterodimer H3s are comprised of distinct “X” and “Y” interaction partners which are altered to prevent either H3 from homodimerizing.

B) Computational models of the designed histone H3 heterodimer. (1) The four-helix bundle comprising the H3-H3 C-terminal dimerization interface (pdb 1kx3). Leucine and alanine residues at the hydrophobic interface are indicated. (2) The designed asymmetric mutations pack efficiently as a heterodimer, with partners colored in green (H3Y) and yellow (H3X). Indicated residues at the H3-H3 interface were engineered to form a bump-hole interface to increase interaction affinity. (3-4) Altered H3s are designed not to homodimerize due to van der Waals clashes (3) or voids (4) in the hydrophobic core.

C-D) Genetic analysis of heterodimeric H3X/H3Y pairs.

C) H3Y alone cannot support growth. Images show growth of yeast carrying wild-type H3 on a *URA3*-marked plasmid as well as either empty plasmid, wild-type H3, H3Y alone, or both H3X and H3Y. Three independent transformants for each strain were grown on 5-FOA to select against the *URA3* shuffle plasmid.

D) H3X alone cannot support growth. Left panels: growth of three independent transformants of various H3X strains (evolved second-generation mutations indicated at left) in the absence of H3Y. Bottom: positive control with a *TRP1*-marked wild-type histone plasmid. Right panels: growth of indicated H3X strains in the presence of H3Y. Synthetic complete (SC) plates were grown 3 days, FOA plates 9 days. No growth on FOA was observed for any of the four evolved H3X alleles in the absence of H3Y, even after extended incubation.

E) Sequences of final H3X-H3Y molecules. All four H3X variants have been validated genetically, while two variants – 126A/130V and 126V/130A – have been validated biochemically (see **Figure 2**). 126A is used for all functional analyses.

Figure 2: Biochemical analysis of asymmetric nucleosome formation in vivo.
A) Schematic for in vivo biochemical analysis of H3X dimerization partner. Yeast strains expressed biotin-tagged H3X along with tagged H3X and H3Y, as indicated.
B) Immunoblot analysis of $H3X^{126A}$ strains. For each of the indicated antibodies (Myc or V5, the same blot was probed sequentially), the left two lanes show total DMS-crosslinked, MNase-digested chromatin (Input), and right lanes show streptavidin-precipitated biotinylated-H3 (Bound). Arrow indicates the expected size (31 kD) of crosslinked H3-H3 dimer species, while asterix indicates monomeric H3 molecules – presence of V5-tagged H3X (left panel) at this position in the bound fraction reflects bead contamination by uncrosslinked H3 molecules. Full gel, including unbound material and DMS control, is shown in **Figure 2 – Figure Supplement 1**.
C) Quantitation of the amounts of the 31kD H3-H3 proteins precipitated with streptavidin-agarose for second-generation H3X variants 126A and 126V. The mean and standard deviation for 3 independent replicate experiments are graphed.

Figure 3: Genetic epistasis between the H3 tails.
(A-B) We constructed 12 sets of point mutations in histone H3, with each mutant cycle including H3X**mut**/H3Ywt, H3Xwt/H3Y**mut**, and H3X**mut**/H3Y**mut** – for each mutant trio, X/Y/double mutations are ordered from left to right, as indicated for the H3R2K mutants. For all 12 trios, as well as the matched "pseudo-wt" (labeled as **pWT**) carrying H3Xwt/H3Ywt (leftmost bar and dashed line), we measured doubling times in at least 6 replicate cultures in low (A) and high (B) KCl. Boxes emphasize H3K14R and H3K36Q trios, as detailed in text.

C-E) Serial dilution growth assay for the indicated strains incubated at 30 C or 34 C, as indicated. Note that yeast carrying pseudo-wild type H3X/H3Y nucleosomes grow poorly at 37C, so we assayed temperature sensitivity at 34 C. Mutant set in (C) shows temperature-sensitivity is specific to symmetric H3K36Q mutant. Mutant set in (D) shows that complete loss of H3K36me3 in the symmetric H3P38V mutant (where H3K36me3 is replaced with H3K36me2) is compatible with rapid growth at high

temperatures. Mutant set in (E) shows that a single dimethylated K36 residue per nucleosome is compatible with rapid growth at high temperatures.

Strains analyzed were: pWT XY (PKY4704), R2K mXY (PKY4749), R2K XmY (PKY4751), R2K mXmY (PKY4753), K9Q mXY (PKY4714), K9Q XmY (PKY4715), K9Q mXmY (PKY4706), K9R mXY (PKY4773), K9R XmY (PKY4775), K9R mXmY (PKY4777), S10A mXY (PKY4716), S10A XmY (PKY4717), S10A mXmY (PKY4707), K14Q mXY (PKY4789), K14Q XmY (PKY4791), K14Q mXmY (PKY4793), K14R mXY (PKY4781), K14R XmY (PKY4783), K14R mXmY (PKY4786), K18Q mXY (PKY4805), K18Q XmY (PKY4807), K18Q mXmY (PKY4809), K18R mXY (PKY4797), K18R XmY (PKY4799), K18R mXmY (PKY4801), K27Q mXY (PKY4822), K27Q XmY (PKY4823), K27Q mXmY (PKY4825), K27R mXY (PKY4813), K27R XmY (PKY4815), K27R mXmY (PKY4817), K36Q mXY (PKY4829), K36Q XmY (PKY4831), K36Q mXmY (PKY4834), K37Q mXY (PKY4837), K37Q XmY (PKY4839), K37Q mXmY (PKY4841), P38V mXY (PKY5033), P38V XmY (PKY5035), P38V mXmY (PKY5037), K36Q mX/P38V mY (PKY5138), and P38V mX/K36Q mY (PKY5140).

pWT XY, pseudo WT; mXY, mutation on X; XmY, mutation on Y; and mXmY, mutation on both X and Y.

Figure 4: Double H3K36Q mutants fail to repress cryptic promoters.

A) Northern blot for *STE11* for RNA isolated from the indicated strains, with 25S Northern shown as a loading control. Top band, which migrates at 2.2 kb, represents the full-length *STE11* transcript, while the two lower molecular-weight bands correspond to previously-characterized sense transcripts initiating within the *STE11* coding region from cryptic promoters (*24*).

B) Quantitation of cryptic transcript levels for *STE11* in the various strains indicated (n=3). Levels of cryptic transcripts were normalized to full-length. Average and std. dev. of triplicate measures of these normalized values are graphed on the y-axes.

Strains analyzed were: WT wt-c (PKY4701), K36Q wt-c (PKY4827), *eaf3Δ* WT wt-c (PKY5077), *eaf3Δ* K36Q wt-c (PKY5079), P38V wt-c (PKY5031), pWT XY (PKY4704), K36Q mXY (PKY4829), K36Q XmY (PKY4831), K36Q mXmY (PKY4834), *eaf3Δ* pWT XY (PKY5081), *eaf3Δ* K36Q mXY (PKY5083), *eaf3Δ* K36Q XmY (PKY5086) and *eaf3Δ* K36Q mXmY (PKY5087), P38V mXY (PKY5033), P38V XmY (PKY5035) and P38V mXmY (PKY5037).

pWT_XY, pseudo wild-type; mXY, mutation on X; XmY, mutation on Y; and mXmY, mutation on both X and Y.

Figure 5: H3S10A affects histone crosstalk in cis.

A) Mass spectrometric analysis of H3X/H3Y heterodimers expressing one biotin-labeled subunit, with a S10A point mutation either located on the same H3 molecule (in cis), or in trans. Left: Schematic of asymmetric nucleosomes. Right: Robust avidin-affinity purification of biotin-labeled H3 molecules. Mass spec quantitation of peptides (described on top of the graphs) from the strains with genotypes indicated on the x-axes. For each peptide, raw peak area scores were normalized by dividing by the peak areas of an internal control, the unmodified H3 peptide containing K42. Average and std. dev. of triplicate measures of these normalized values are graphed on the y-axes. As expected, S10A-containing peptides were only detected when present in cis on the biotin-labeled histone, but not when expressed in trans on the heterodimeric partner.

B) H3K9 acetylation levels are diminished in cis in H3S10A mutants. Data are shown for mass spec analysis of the indicated mutant strains. Left two bars show data for wild-type and double H3S10A mutants on the background of a wild-type H3-H3 interface. Right four panels show H3K9Ac levels on an avidin-purified biotin-tagged H3 molecule, showing data for H3X acetylation in the context of the pseudo-wild type H3X/Y background, H3X acetylation on the same (cis) or opposite tail from an H3S10A mutation, and H3X acetylation in a double H3XS10A/H3YS10A mutant.

C) Western blots confirming effects of symmetric S10A on K9 acetylation both on the WT H3-H3 background, and on the X-Y background, as indicated. For the right panel, the epitope tag present on H3X allows separate probing of the H3X and H3Y molecules. Total protein on blots was visualized by Ponceau S staining. Note that although the S10A mutation in principle might affect anti-H3K9ac antibody (Abcam ab10812) binding, these results are highly concordant with the mass spectrometry measurements in panel (B), where the ability to detect lysine acetylation (based on peptide mass) is unaffected by the difference between S10 and S10A.

D-F) Quantitation of blots from panel (C). K9Ac signals were normalized to total protein detected by Ponceau S.

Strains analyzed were: WT wt-C (PKY4610), S10A wt-C (PKY5003), pWT-XY (PKY4983), S10A-XY-cis (PKY5005), S10A-XY trans (PKY4986) and S10A-XY double (PKY5042).

SUPPLEMENTAL MATERIALS

Supplementary File 1

Figure 1-figure supplement 1

Figure 2-figure supplement 1

Figure 3-figure supplements 1-2

Figure 4-figure supplement 1

SUPPLEMENTARY FILES

Supplementary Table 1. Yeast strain list.

SUPPLEMENTAL FIGURE LEGENDS

Figure 1-figure supplement 1

Optimization of the H3X/H3Y design.

A) Genetic analysis of the original H3X design. The top four panels are identical to **Figure 1C**, showing growth of H3X/H3Y-bearing yeast strains but no growth of H3Y-bearing strains, and are duplicated here for comparison to H3X growth phenotypes. Bottom two panels: Yeast bearing a wild type histone-*URA3* shuffle plasmid were transfected with the indicated plasmids carrying a wild-type H4 gene and the original

H3X (126V, 130V) gene. Three independent isolates of each strain were patched onto 5-FOA media to select for loss of the wild type histone-*URA3* plasmid. Strains were grown for the indicated number of days and photographed. The growth of papillae in the absence of H3Y upon extended incubation led us to optimize H3X by randomization of four key residues, as shown below.

B) Sequencing traces for the four "H3X*" libraries, each with one randomly mutagenized codon as indicated. Although the base utilization in the synthetic oligonucleotides is not completely equal, all four bases are readily detected at each position.

C) Schematic of the screening strategy. Transformants carrying the H3X* library alleles were plated on SC-Trp and replicated onto FOA plates. Strains that couldn't survive on FOA with H3* alone were transformed with an H3Y-expressing plasmid, and then were tested on FOA media to assess the viability of the H3X*-H3Y combinations (as shown in **Figure 1C**). As an additional criterion, we tested whether the two plasmids expressing the new H3X/H3Y heterodimers were stable when cells were cultured in rich media in the absence of selection for either plasmid. Repeated rounds of streaking on rich (YPD) plates or culturing in YPD media yielded colonies that all maintained a $Trp^{+}Leu^{+}$ phenotype, indicating that neither plasmid could be lost. Furthermore, resequencing of plasmids isolated after growth on YPD detected no reversion of the engineered H3X or H3Y in 96 independent isolates. Together, the genetic data strongly suggested that the H3X/H3Y combinations are obligate heterodimers, and that neither H3X nor H3Y can homodimerize at sufficient levels to support viability.

Figure 2-figure supplement 1

Western blot analysis of asymmetric nucleosome formation in vivo.

Immunoblot analysis of Biotin-$H3X^{126A}$ strains. Lanes 3-4 and 7-8 from these gels are reproduced **Figure 2B, E**. Lanes 1-2: whole cell extracts after 0 or 60 minutes of DMS crosslinking. Lanes 3-8: DMS-crosslinked, MNase-digested chromatin from the indicated strains was precipitated with streptavidin-agarose to capture biotinylated (Bio) H3. I=Input, U= Unbound: 0.75% and 1.5% of total shown in adjacent lanes; B = Bound: 10 and 20% of total shown. Proteins were separated by 17% SDS-PAGE, transferred to a membrane, and probed sequentially with the indicated primary antibodies. Arrow

indicates the expected size of crosslinked H3-H3 dimer species, while asterix indicates monomeric H3 molecules – presence of V5-tagged H3X (left panel) at this position in the bound fraction reflects bead contamination by uncrosslinked H3 molecules.

Figure 3-figure supplement 1

Significant growth defects for the H3K36Q double mutant, relative to either single mutant.

Dot plots show all growth rates in 0.8M KCl for all individual replicate time courses for the indicated H3K36Q mutants.

Figure 3-figure supplement 2

Temperature sensitivity of various histone mutant strains.

For all panels, serial dilutions of the indicated strains were plated at 30 C, 34 C, or 37 C, as indicated.

A) Data for WT wt-c (PKY4701), K36Q wt-c (PKY4827), P38V wt-c (PKY5031), *eaf3Δ* WT wt-c (PKY5077) and *eaf3Δ* K36Q wt-c (PKY5079).

B) Data for WT wt-c (PKY4701), K14R wt-c (PKY4779), K14Q wt-c (PKY4787) and K56R wt-c (PKY4843).

C) Data for pWT XY (PKY4704), *eaf3Δ* pWT XY (PKY5081), *eaf3Δ* K36Q mXY (PKY5083), *eaf3Δ* K36Q XmY (PKY5086) and *eaf3Δ* K36Q mXmY (PKY5087).

D) Data for pWT XY (PKY4704), K14R mXY (PKY4781), K14R XmY (PKY4783) and K14R mXmY (PKY4786).

E) Data for pWT XY (PKY4704), K14Q mXY (PKY4789), K14Q XmY (PKY4791) and K14Q mXmY (PKY4793)

pWT_XY, pseudo WT; mXY, mutation on X; XmY, mutation on Y; and mXmY, mutation on both X and Y.

Figure 4-figure supplement 1

Effects of H3K36Q mutants on cryptic transcription.

As in **Figure 4**, with *FLO8* used as a probe for Northern blots in place of *STE11*.

REFERENCES

1. N. Friedman, O. J. Rando, Epigenomics and the structure of the living genome. *Genome research* **25**, 1482-1490 (2015).
2. R. D. Kornberg, Y. Lorch, Twenty-five years of the nucleosome, fundamental particle of the eukaryote chromosome. *Cell* **98**, 285-294 (1999).
3. P. Voigt *et al.*, Asymmetrically modified nucleosomes. *Cell* **151**, 181-193 (2012).
4. E. Shema *et al.*, Single-molecule decoding of combinatorially modified nucleosomes. *Science (New York, N.Y* **352**, 717-721 (2016).
5. H. S. Rhee, A. R. Bataille, L. Zhang, B. F. Pugh, Subnucleosomal Structures and Nucleosome Asymmetry across a Genome. *Cell* **159**, 1377-1388 (2014).
6. S. Ramachandran, G. E. Zentner, S. Henikoff, Asymmetric nucleosomes flank promoters in the budding yeast genome. *Genome research* **25**, 381-390 (2015).
7. S. Li, M. A. Shogren-Knaak, Cross-talk between histone H3 tails produces cooperative nucleosome acetylation. *Proceedings of the National Academy of Sciences of the United States of America* **105**, 18243-18248 (2008).
8. S. Li, M. A. Shogren-Knaak, The Gcn5 bromodomain of the SAGA complex facilitates cooperative and cross-tail acetylation of nucleosomes. *The Journal of biological chemistry* **284**, 9411-9417 (2009).
9. S. L. Mayo, B. D. Olafson, W. A. Goddard, DREIDING: a generic force field for molecular simulations. *J Phys Chem* **94**, 8897-8909 (1990).
10. D. N. Bolon, R. A. Grant, T. A. Baker, R. T. Sauer, Specificity versus stability in computational protein design. *Proceedings of the National Academy of Sciences of the United States of America* **102**, 12724-12729 (2005).
11. J. Dai *et al.*, Probing nucleosome function: a highly versatile library of synthetic histone H3 and H4 mutants. *Cell* **134**, 1066-1078 (2008).
12. D. Beckett, E. Kovaleva, P. J. Schatz, A minimal peptide substrate in biotin holoenzyme synthetase-catalyzed biotinylation. *Protein Sci* **8**, 921-929 (1999).
13. R. D. Kornberg, J. O. Thomas, Chromatin structure; oligomers of the histones. *Science (New York, N.Y* **184**, 865-868 (1974).
14. J. O. Thomas, Chemical cross-linking of histones. *Methods Enzymol* **170**, 549-571 (1989).
15. A. Weiner *et al.*, Systematic dissection of roles for chromatin regulators in a yeast stress response. *PLoS biology* **10**, e1001369 (2012).
16. B. D. Strahl *et al.*, Set2 is a nucleosomal histone H3-selective methyltransferase that mediates transcriptional repression. *Molecular and cellular biology* **22**, 1298-1306 (2002).
17. M. J. Carrozza *et al.*, Histone H3 methylation by Set2 directs deacetylation of coding regions by Rpd3S to suppress spurious intragenic transcription. *Cell* **123**, 581-592 (2005).
18. M. C. Keogh *et al.*, Cotranscriptional set2 methylation of histone H3 lysine 36 recruits a repressive Rpd3 complex. *Cell* **123**, 593-605 (2005).
19. A. A. Joshi, K. Struhl, Eaf3 chromodomain interaction with methylated H3-K36 links histone deacetylation to Pol II elongation. *Molecular cell* **20**, 971-978 (2005).
20. C. K. Govind *et al.*, Phosphorylated Pol II CTD recruits multiple HDACs, including Rpd3C(S), for methylation-dependent deacetylation of ORF nucleosomes. *Molecular cell* **39**, 234-246 (2010).

21. J. W. Huh *et al.*, Multivalent di-nucleosome recognition enables the Rpd3S histone deacetylase complex to tolerate decreased H3K36 methylation levels. *The EMBO journal* **31**, 3564-3574 (2012).
22. C. J. Nelson, H. Santos-Rosa, T. Kouzarides, Proline isomerization of histone H3 regulates lysine methylation and gene expression. *Cell* **126**, 905-916 (2006).
23. M. L. Youdell *et al.*, Roles for Ctk1 and Spt6 in regulating the different methylation states of histone H3 lysine 36. *Molecular and cellular biology* **28**, 4915-4926 (2008).
24. C. D. Kaplan, L. Laprade, F. Winston, Transcription elongation factors repress transcription initiation from cryptic sites. *Science (New York, N.Y* **301**, 1096-1099 (2003).
25. T. Suganuma, J. L. Workman, Crosstalk among Histone Modifications. *Cell* **135**, 604-607 (2008).
26. W. S. Lo *et al.*, Phosphorylation of serine 10 in histone H3 is functionally linked in vitro and in vivo to Gcn5-mediated acetylation at lysine 14. *Molecular cell* **5**, 917-926 (2000).
27. L. M. Johnson, P. S. Kayne, E. S. Kahn, M. Grunstein, Genetic evidence for an interaction between SIR3 and histone H4 in the repression of the silent mating loci in Saccharomyces cerevisiae. *Proceedings of the National Academy of Sciences of the United States of America* **87**, 6286-6290 (1990).
28. D. Segre, A. Deluna, G. M. Church, R. Kishony, Modular epistasis in yeast metabolism. *Nature genetics* **37**, 77-83 (2005).
29. S. A. Morris *et al.*, Identification of histone H3 lysine 36 acetylation as a highly conserved histone modification. *The Journal of biological chemistry* **282**, 7632-7640 (2007).
30. A. Sawicka, C. Seiser, Sensing core histone phosphorylation - a matter of perfect timing. *Biochimica et biophysica acta* **1839**, 711-718 (2014).
31. D. J. McKay *et al.*, Interrogating the function of metazoan histones using engineered gene clusters. *Developmental cell* **32**, 373-386 (2015).
32. M. F. Dion *et al.*, Dynamics of replication-independent histone turnover in budding yeast. *Science (New York, N.Y* **315**, 1405-1408 (2007).
33. J. Recht *et al.*, Histone chaperone Asf1 is required for histone H3 lysine 56 acetylation, a modification associated with S phase in mitosis and meiosis. *Proceedings of the National Academy of Sciences of the United States of America* **103**, 6988-6993 (2006).
34. B. MacLean *et al.*, Skyline: an open source document editor for creating and analyzing targeted proteomics experiments. *Bioinformatics* **26**, 966-968 (2010).
35. M. A. Collart, S. Oliviero, Preparation of yeast RNA. *Curr Protoc Mol Biol* **Chapter 13**, Unit13 12 (2001).
36. N. Morohashi *et al.*, Effect of sequence-directed nucleosome disruption on cell-type-specific repression by alpha2/Mcm1 in the yeast genome. *Eukaryot Cell* **5**, 1925-1933 (2006).
37. S. G. Pattenden, M. M. Gogol, J. L. Workman, Features of cryptic promoters and their varied reliance on bromodomain-containing factors. *PloS one* **5**, e12927 (2010).

Figure 1

A

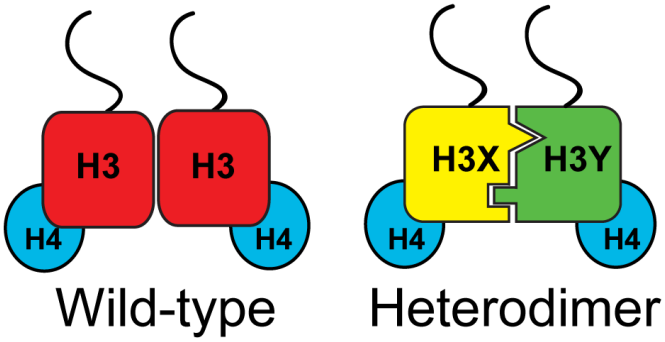

C

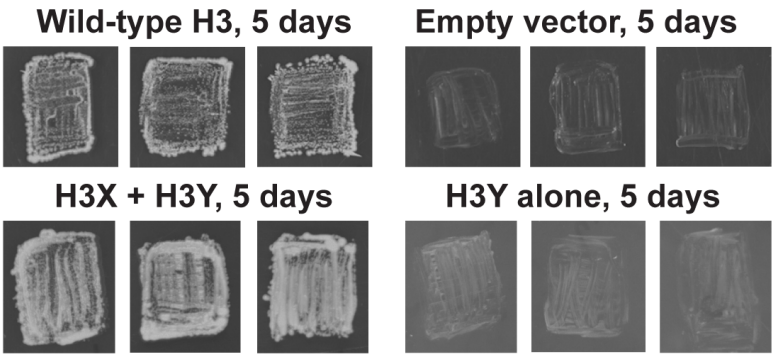

B

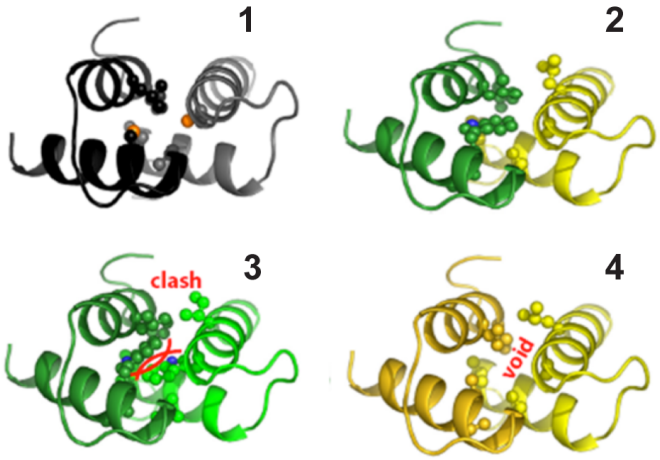

D

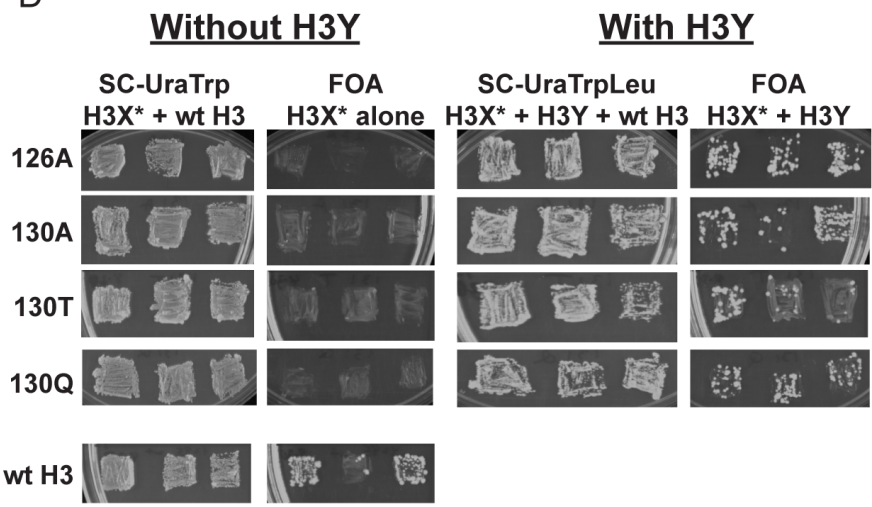

E

4 sequences genetically selected:

L126A, L130V
L126V, L130A
L126V, L130T
L126V, L130Q

1 computationally designed:

L109I, A110W, L130I

Figure 1 Supplement 1

A

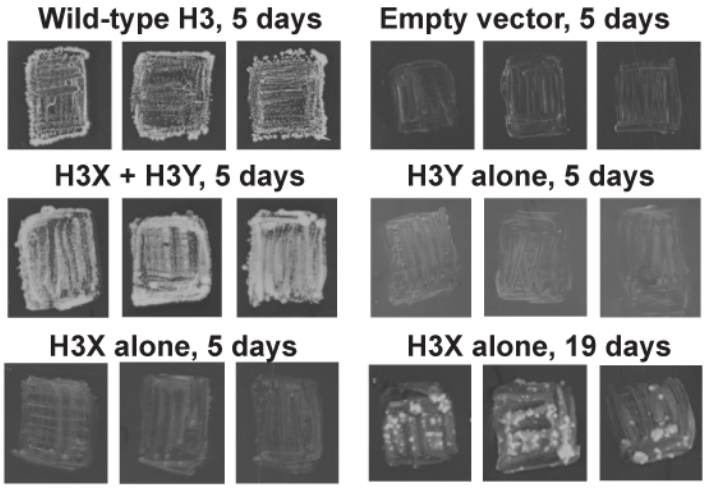

B

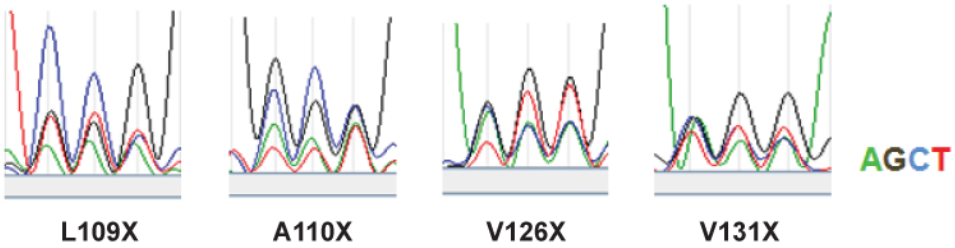

C

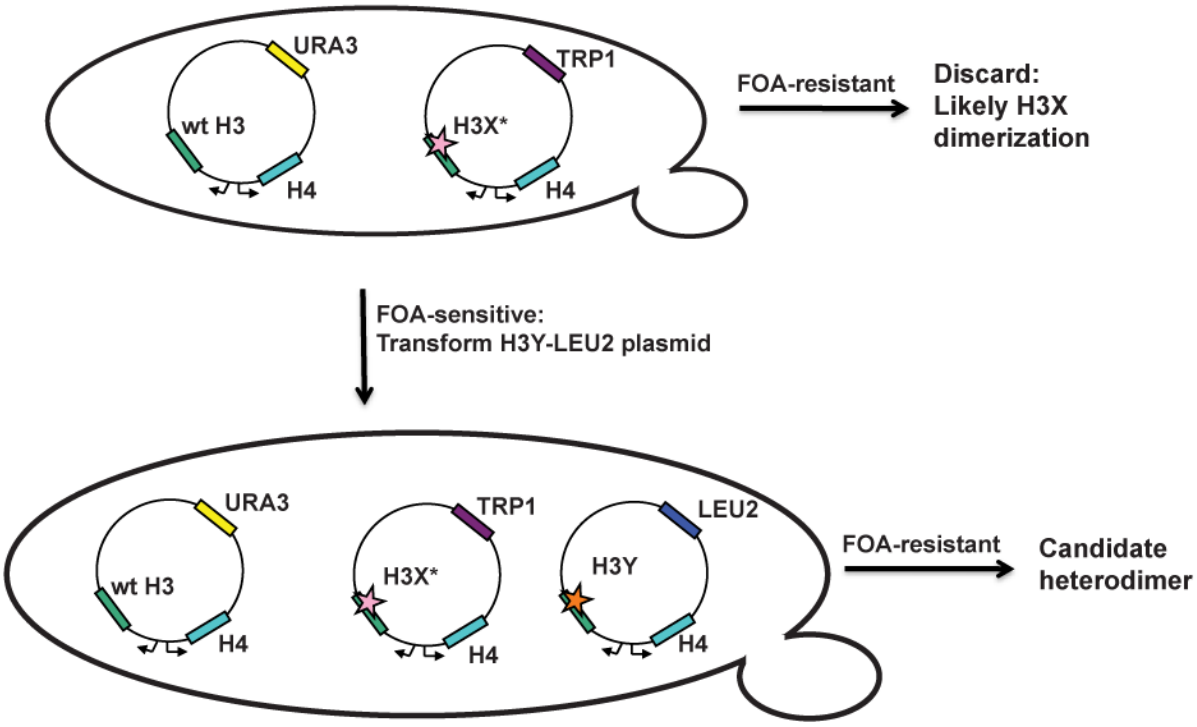

Figure 2

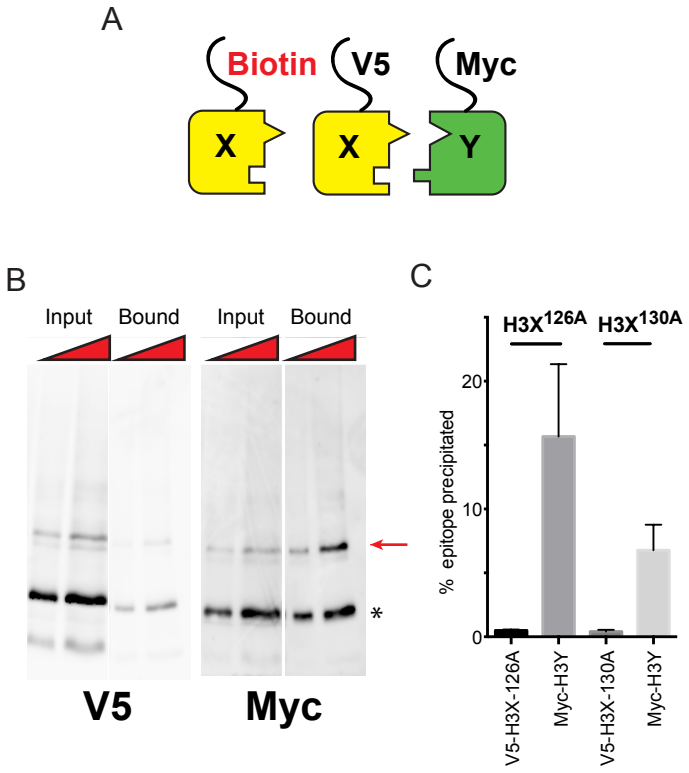
A
Biotin
V5
Myc
X
X
Y
B
Input
Bound
Input
Bound
*
V5
Myc
C
H3X126A
H3X130A
% epitope precipitated
20
10
0
V5-H3X-126A
Myc-H3Y
V5-H3X-130A
Myc-H3Y

Figure 2 Supplement 1

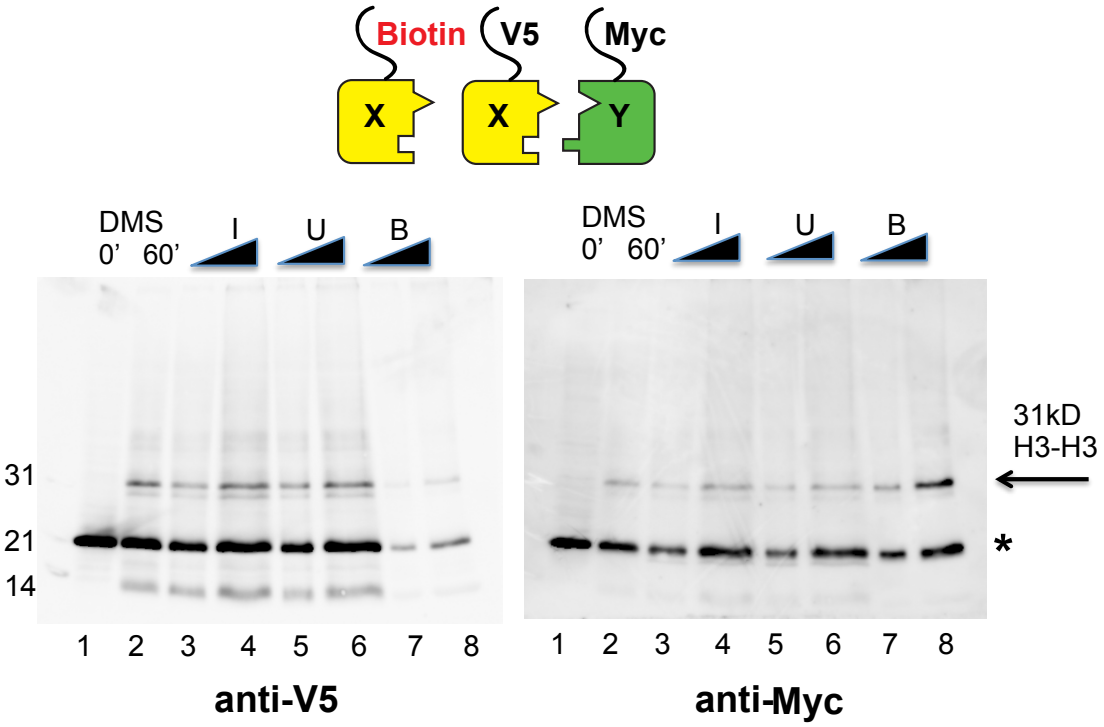

Figure 3

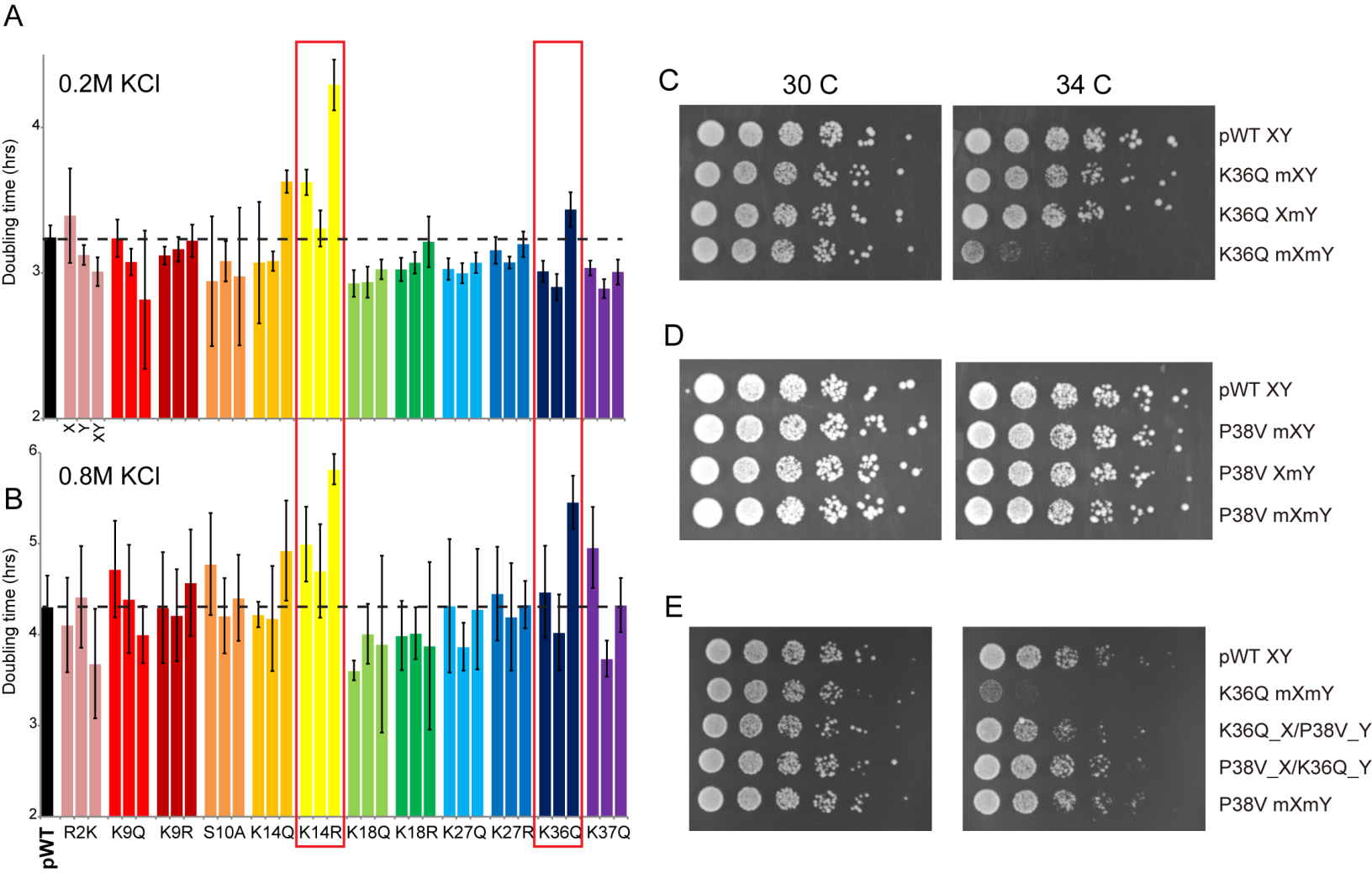
A
0.2M KCl
Doubling time (hrs)
X
Y
XY
B
0.8M KCl
Doubling time (hrs)
pWT
R2K
K9Q
K9R
S10A
K14Q
K14R
K18Q
K18R
K27Q
K27R
K36Q
K37Q
C
30 C
34 C
pWT XY
K36Q mXY
K36Q XmY
K36Q mXmY
D
pWT XY
P38V mXY
P38V XmY
P38V mXmY
E
pWT XY
K36Q mXmY
K36Q_X/P38V_Y
P38V_X/K36Q_Y
P38V mXmY

Figure 3 Supplement 1

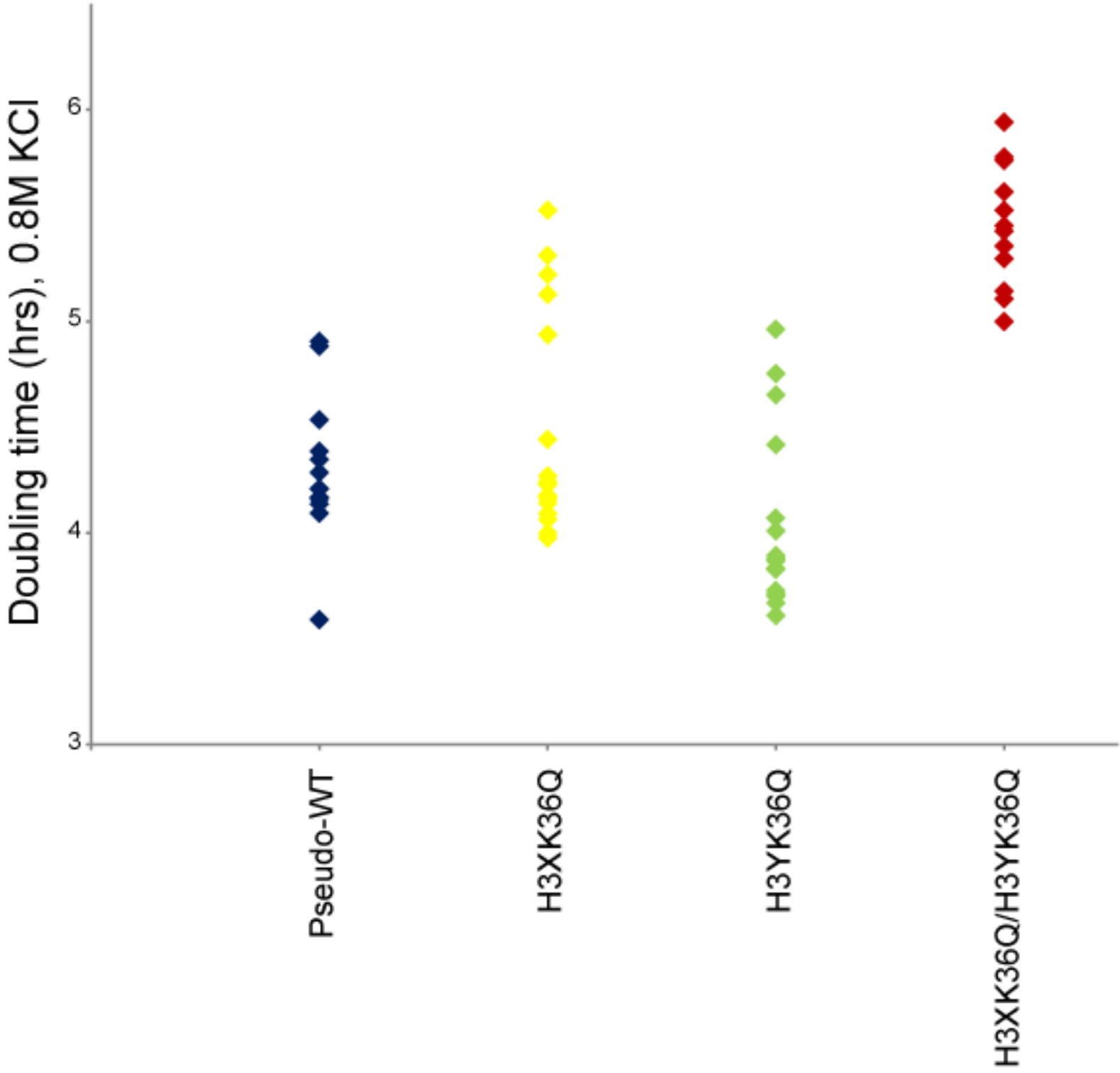

Figure 3 Supplement 2

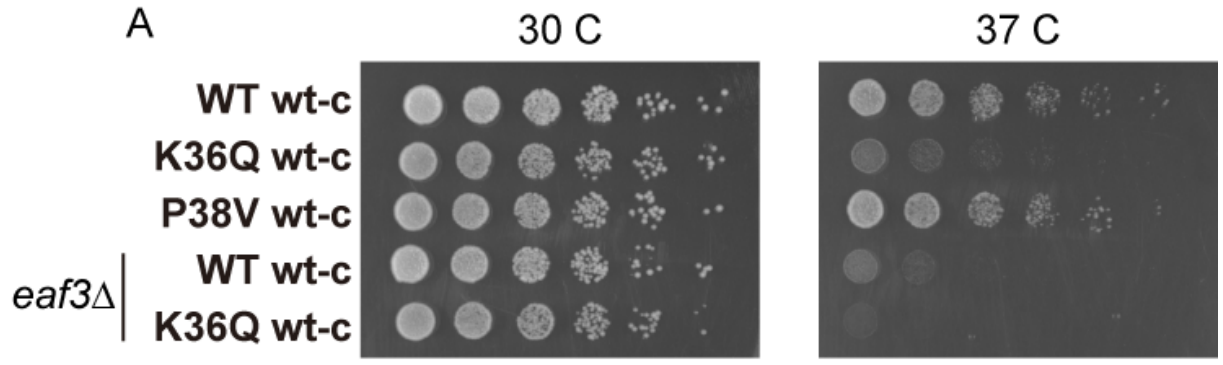

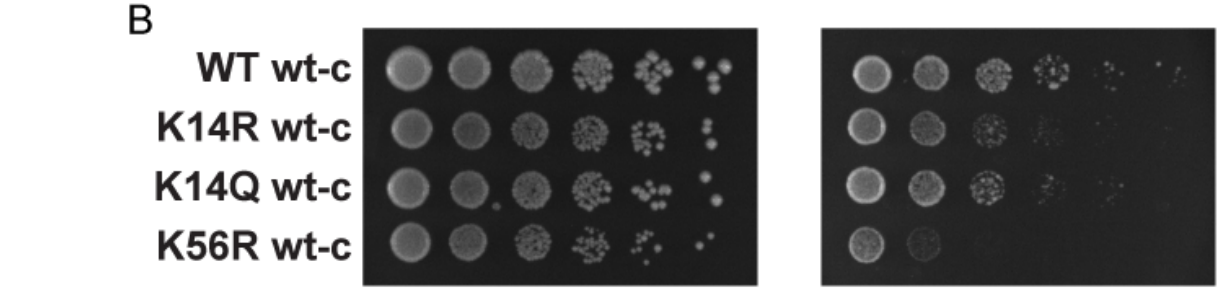

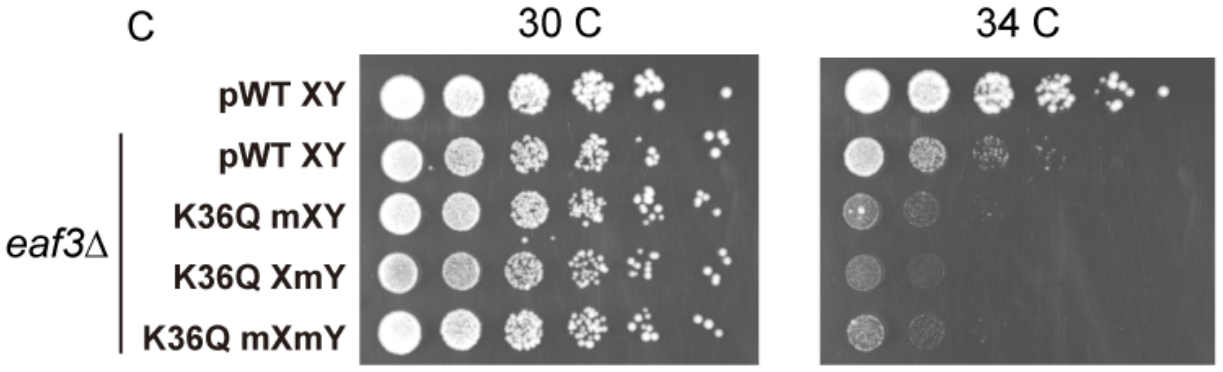

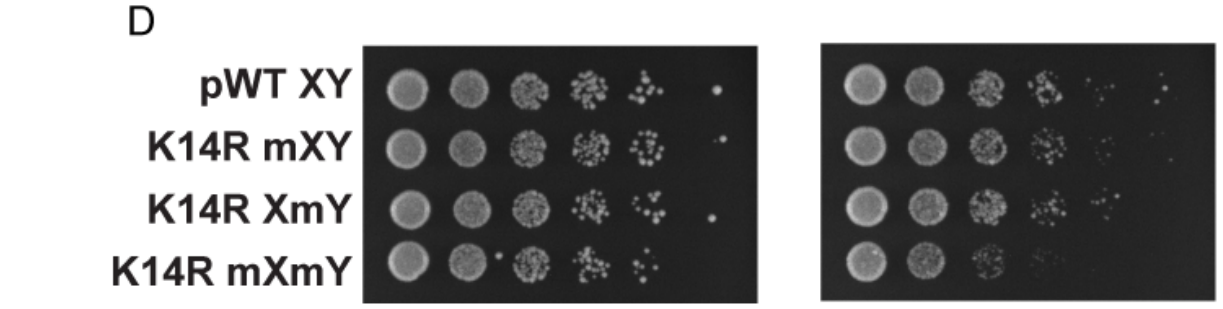

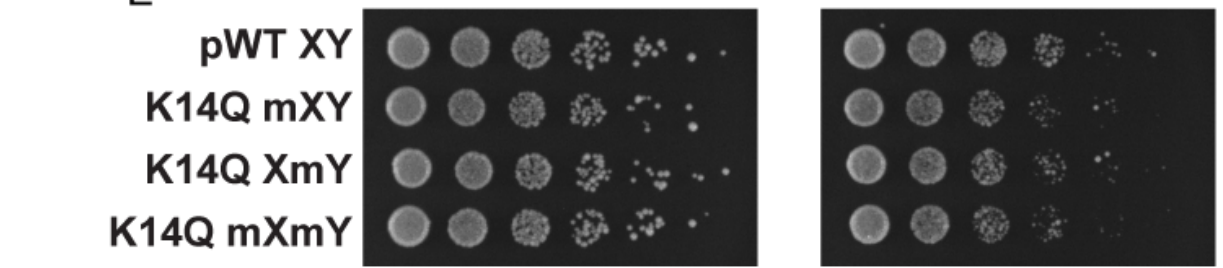

Figure 4

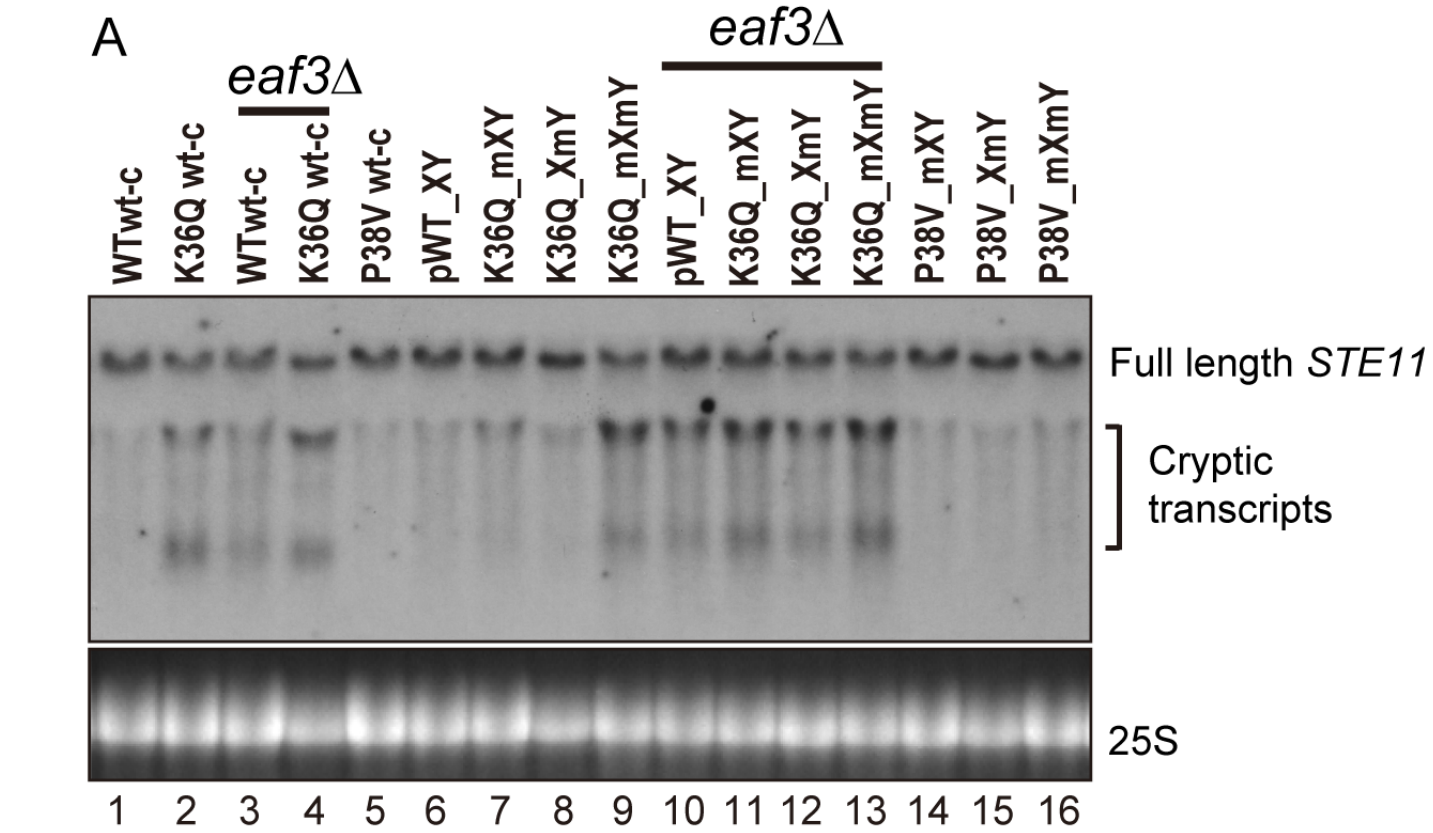
A
eaf3Δ
eaf3Δ
WTwt-c
K36Q wt-c
WTwt-c
K36Q wt-c
P38V wt-c
pWT_XY
K36Q_mXY
K36Q_XmY
K36Q_mXmY
pWT_XY
K36Q_mXY
K36Q_XmY
K36Q_mXmY
P38V_mXY
P38V_XmY
P38V_mXmY
Full length STE11
Cryptic transcripts
25S
1 2 3 4 5 6 7 8 9 10 11 12 13 14 15 16

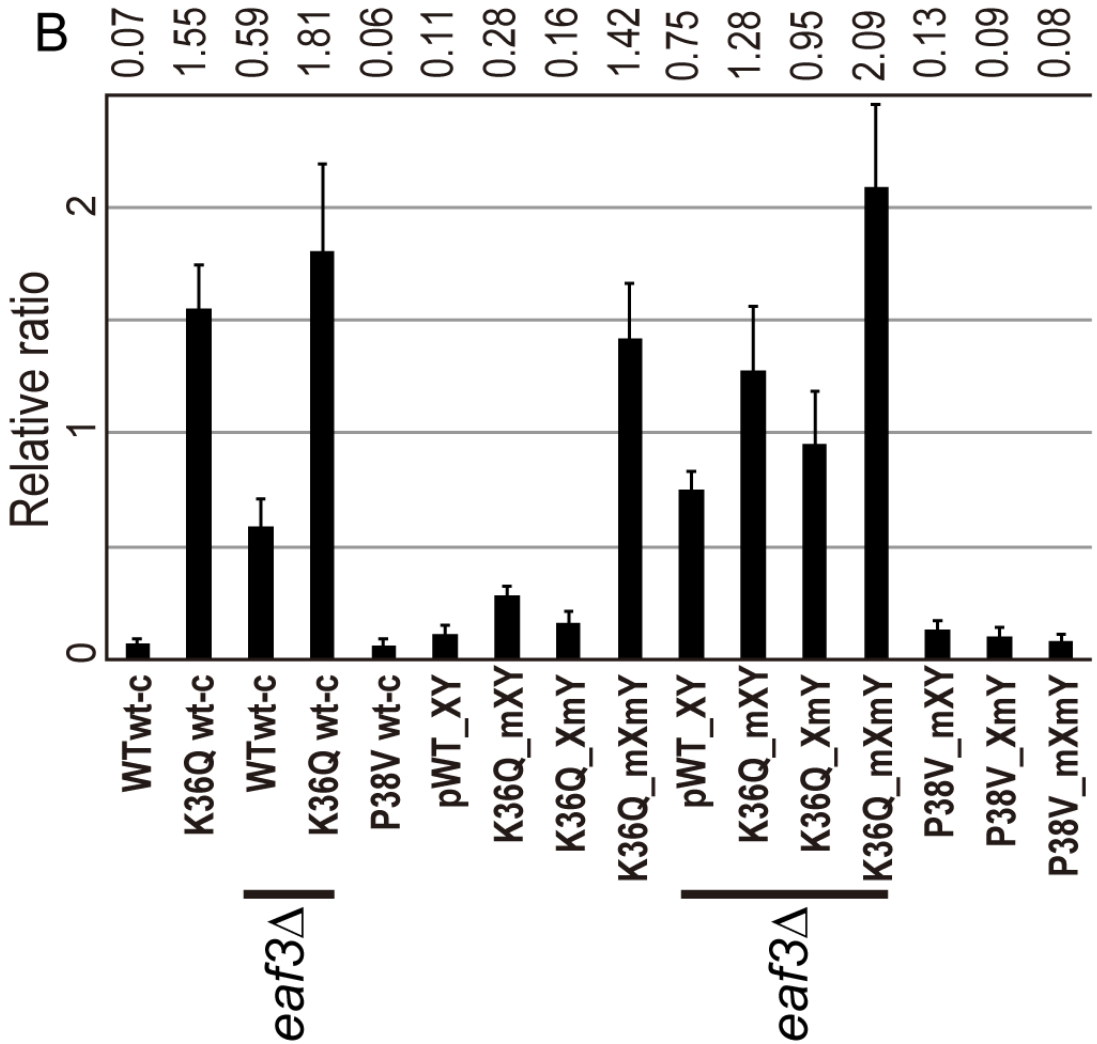
B
0.07 1.55 0.59 1.81 0.06 0.11 0.28 0.16 1.42 0.75 1.28 0.95 2.09 0.13 0.09 0.08
Relative ratio
0
1
2
WTwt-c
K36Q wt-c
WTwt-c
K36Q wt-c
P38V wt-c
pWT_XY
K36Q_mXY
K36Q_XmY
K36Q_mXmY
pWT_XY
K36Q_mXY
K36Q_XmY
K36Q_mXmY
P38V_mXY
P38V_XmY
P38V_mXmY
eaf3Δ
eaf3Δ

Figure 4 Supplement 1

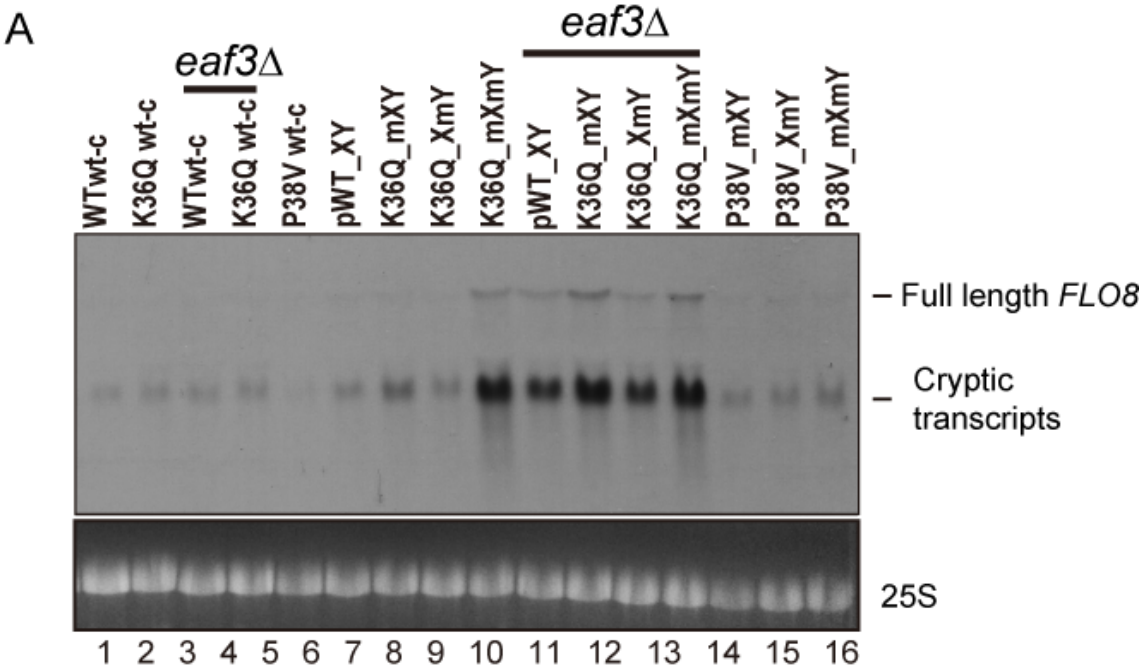

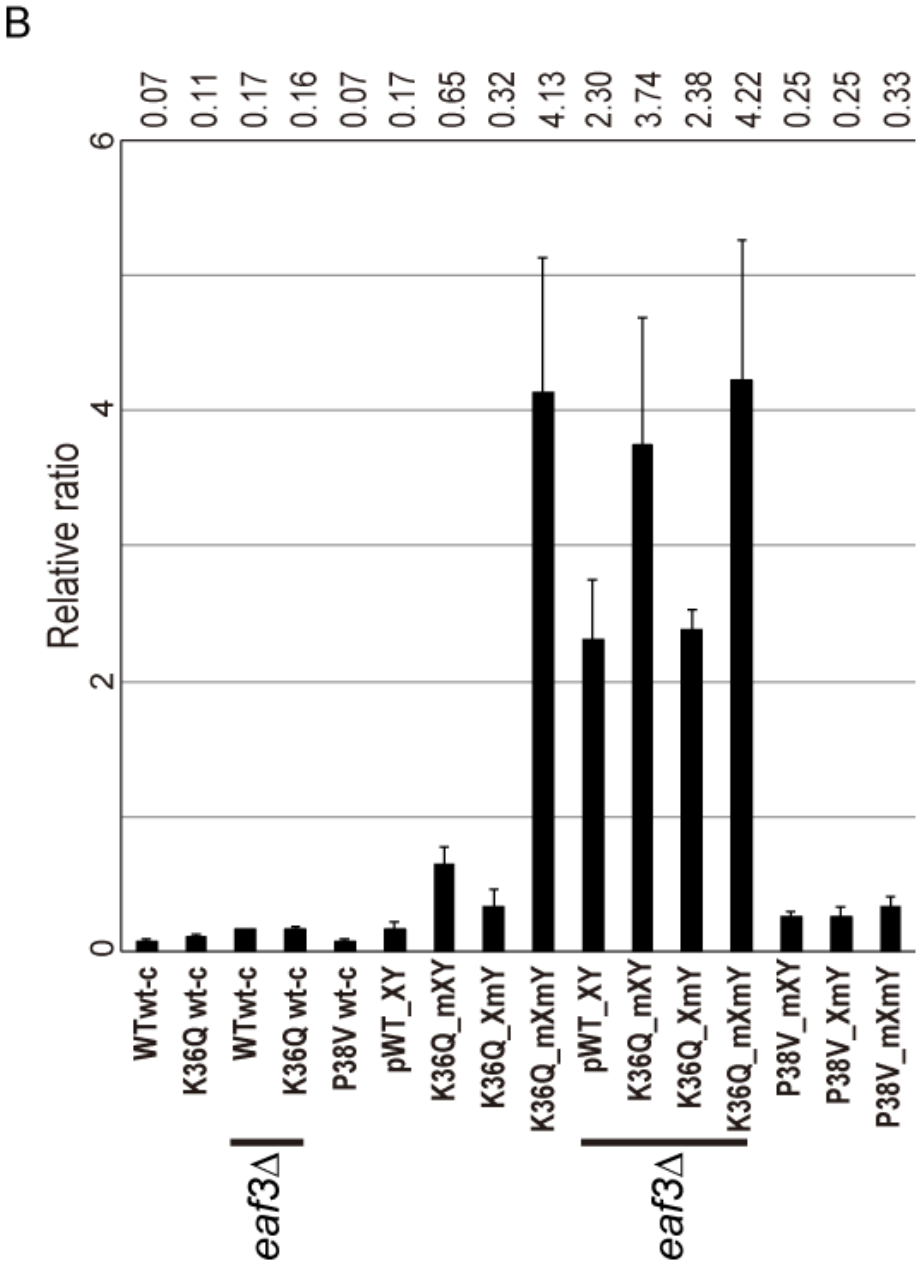

Figure 5

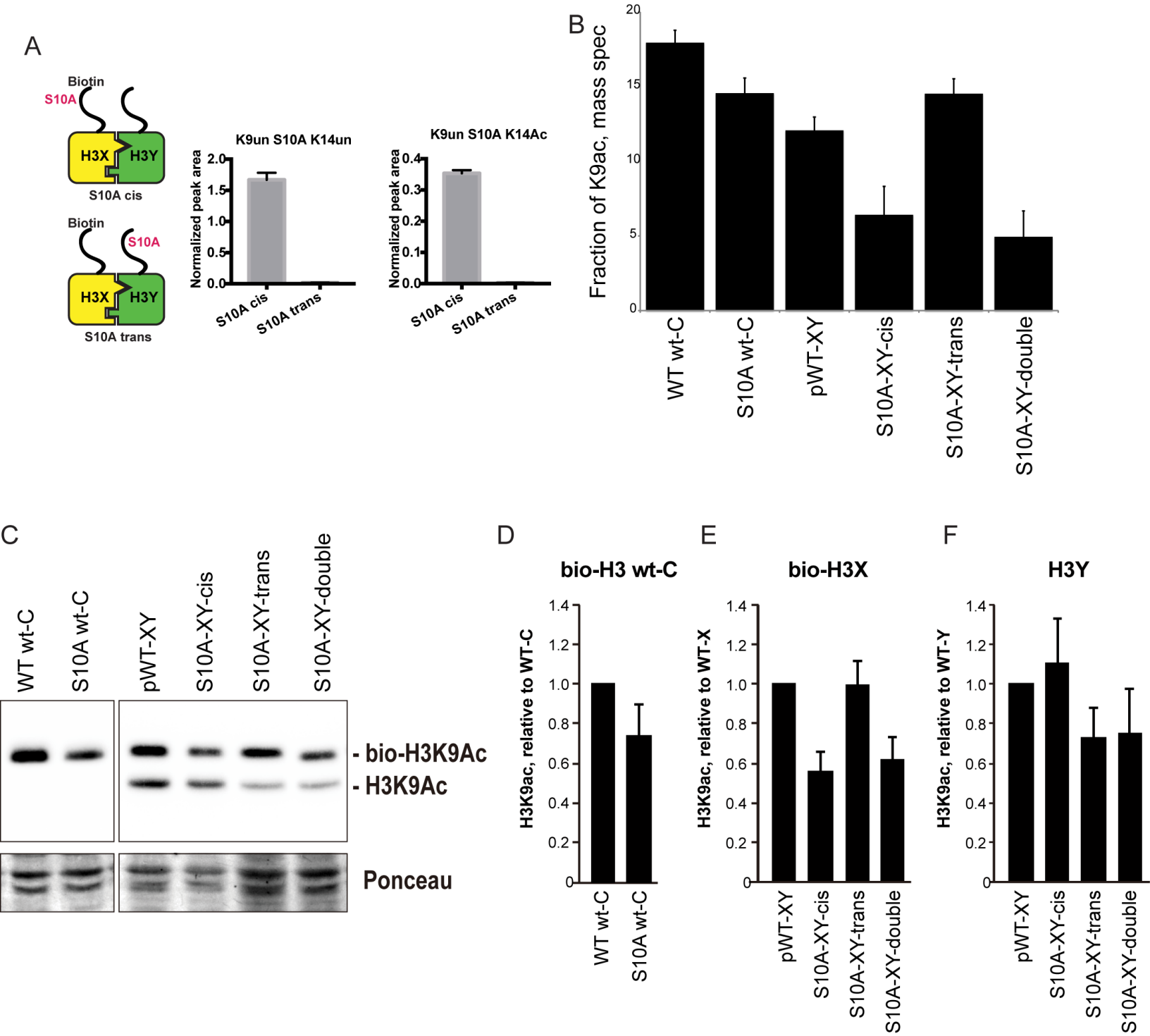
A
Biotin
S10A
H3X
H3Y
S10A cis
Biotin
S10A
H3X
H3Y
S10A trans
K9un S10A K14un
Normalized peak area
2.0
1.5
1.0
0.5
0.0
S10A cis
S10A trans
K9un S10A K14Ac
Normalized peak area
0.4
0.3
0.2
0.1
0.0
S10A cis
S10A trans
B
Fraction of K9ac, mass spec
20
15
10
5
0
WT wt-C
S10A wt-C
pWT-XY
S10A-XY-cis
S10A-XY-trans
S10A-XY-double
C
WT wt-C
S10A wt-C
pWT-XY
S10A-XY-cis
S10A-XY-trans
S10A-XY-double
- bio-H3K9Ac
- H3K9Ac
Ponceau
D
bio-H3 wt-C
H3K9ac, relative to WT-C
1.4
1.2
1.0
0.8
0.6
0.4
0.2
0
WT wt-C
S10A wt-C
E
bio-H3X
H3K9ac, relative to WT-X
1.4
1.2
1.0
0.8
0.6
0.4
0.2
0
pWT-XY
S10A-XY-cis
S10A-XY-trans
S10A-XY-double
F
H3Y
H3K9ac, relative to WT-Y
1.4
1.2
1.0
0.8
0.6
0.4
0.2
0
pWT-XY
S10A-XY-cis
S10A-XY-trans
S10A-XY-double

Strain list

Strain	Description	Parent	Reference
PKY4171	MAT**a**; Δ(*hht1-hhf1*); Δ(*hht2-hhf2*); *leu2-3,112*; *ura3-62*; *trp1*; *his3*; *bar1::hisG+ p(HHT1-HHF1, URA3, CEN)*	MSY421	(Recht *et al.* PNAS 2006)
PKY4625	+ P22 (Myc-H3Y = Myc-hht2(L109I, A110W, L130I), HHF2, LEU2) + P67 (bio-H3X-126A = biotin-hht2(L126A, L130V), HHF2, TRP1) + P72 (V5-H3X-126A = V5-hht2(L126A, L130V), HHF2, URA3)	PKY4171	This study (Fig. 2)
PKY4626	+ P22 (Myc-H3Y = Myc-hht2(L109I, A110W, L130I), HHF2, LEU2) + P71 (bio-H3X-130A = biotin-hht2(L126V, L130A), HHF2, TRP1) + P73 (V5-H3X-130A = V5-hht2(L126V, L130A), HHF2, URA3)	PKY4171	This study (Fig. 2)
PKY4694	+ P54 (biotin-H3Y = biotin-hht2(L109I, A110W, L130I), HHF2, LEU2) + P72 (V5-126A = V5-hht2(L126A, L130V), HHF2, URA3) + P35 (Myc-H3Y = Myc-hht2(L109I, A110W, L130I), HHF2, TRP1)	PKY4171	This study (Fig. 2)
PKY4695	+ P54 (biotin-H3Y = biotin-hht2(L109I, A110W, L130I), HHF2, LEU2) + P73 (V5-130A = V5-hht2(L126V, L130A), HHF2, URA3) + P35 (Myc-H3Y = Myc-hht2(L109I, A110W, L130I), HHF2, TRP1)	PKY4171	This study (Fig. 2)
PKY4701 (WT wt-c)	MAT**a**; Δ(*hht-hhf1*); Δ(*hht2-hhf2*); *leu2-3,112*; *ura3-62*; *trp1*; *his3*; + pPK188 (HHT2-HHF2, URA3, CEN)	PKY4130	This study (Fig. 3-S2, 4)
PKY4704 (pWT XY)	+pH3X (H3X = hht2(L126A, L130V), HHF2, TRP1) +pH3Y (H3Y = hht2(L109I, A110W, L130I), HHF2, LEU2)	PKY4701	This study (Fig. 3, 4)
PKY4749 (R2K mXY)	+P93 (H3X-R2K = hht2(R2K, L126A, L130V), HHF2, TRP1) + pH3Y (H3Y = hht2(L109I, A110W, L130I), HHF2, LEU2)	PKY4701	This study (Fig. 3)
PKY4751 (R2K XmY)	+ pH3X (H3X = hht2(L126A, L130V), HHF2, TRP1) +P94 (H3Y-R2K = hht2(R2K, L109I, A110W, L130I), HHF2, LEU2)	PKY4701	This study (Fig. 3)
PKY4753 (R2K mXmY)	+P93 (H3X-R2K = hht2(R2K, L126A, L130V), HHF2, TRP1) +P94 (H3Y-R2K = hht2(R2K, L109I, A110W, L130I), HHF2, LEU2)	PKY4701	This study (Fig. 3)
PKY4714 (K9Q mXY)	+P81 (H3X-K9Q = hht2(K9Q, L126A, L130V), HHF2, TRP1) + pH3Y (H3Y = hht2(L109I, A110W, L130I), HHF2, LEU2)	PKY4701	This study (Fig. 3)
PKY4715 (K9Q XmY)	+ pH3X (H3X = hht2(L126A, L130V), HHF2, TRP1) +P84 (H3Y-K9Q = hht2(K9Q, L109I, A110W, L130I), HHF2, LEU2)	PKY4701	This study (Fig. 3)
PKY4706 (K9Q mXmY)	+P81 (H3X-K9Q = hht2(K9Q, L126A, L130V), HHF2, TRP1) +P84 (H3Y-K9Q = hht2(K9Q, L109I, A110W, L130I), HHF2, LEU2)	PKY4701	This study (Fig. 3)

PKY4773 (K9R mXY)	+P102 (H3X-K9R = hht2(K9R, L126A, L130V), HHF2, TRP1) + pH3Y (H3Y = hht2(L109I, A110W, L130I), HHF2, LEU2)	PKY4701	This study (Fig. 3)
PKY4775 (K9R XmY)	+ pH3X (H3X = hht2(L126A, L130V), HHF2, TRP1) +P103 (H3Y-K9R = hht2(K9R, L109I, A110W, L130I), HHF2, LEU2)	PKY4701	This study (Fig. 3)
PKY4777 (K9R mXmY)	+P102 (H3X-K9R = hht2(K9R, L126A, L130V), HHF2, TRP1) +P103 (H3Y-K9R = hht2(K9R, L109I, A110W, L130I), HHF2, LEU2)	PKY4701	This study (Fig. 3)
PKY4716 (S10A mXY)	+P82 (H3X-S10A = hht2(S10A, L126A, L130V), HHF2, TRP1) + pH3Y (H3Y = hht2(L109I, A110W, L130I), HHF2, LEU2)	PKY4701	This study (Fig. 3)
PKY4717 (S10A XmY)	+ pH3X (H3X = hht2(L126A, L130V), HHF2, TRP1) +P85 (H3Y-S10A = hht2(S10A, L109I, A110W, L130I), HHF2, LEU2)	PKY4701	This study (Fig. 3)
PKY4707 (S10A mXmY)	+P82 (H3X-S10A = hht2(S10A, L126A, L130V), HHF2, TRP1) +P85 (H3Y-S10A = hht2(S10A, L109I, A110W, L130I), HHF2, LEU2)	PKY4701	This study (Fig. 3)
PKY4787 (K14Q wt-c)	+ p107 (H3-K14Q = hht2(K14Q), HHF2, TRP1) +pRS415	PKY4701	This study (Fig. 3-S2)
PKY4789 (K14Q mXY)	+P108 (H3X-K14Q = hht2(K14Q, L126A, L130V), HHF2, TRP1) + pH3Y (H3Y = hht2(L109I, A110W, L130I), HHF2, LEU2)	PKY4701	This study (Fig. 3)
PKY4791 (K14Q XmY)	+ pH3X (H3X = hht2(L126A, L130V), HHF2, TRP1) +P109 (H3Y-K14Q = hht2(K14Q, L109I, A110W, L130I), HHF2, LEU2)	PKY4701	This study (Fig. 3)
PKY4793 (K14Q mXmY)	+P108 (H3X-K14Q = hht2(K14Q, L126A, L130V), HHF2, TRP1) +P109 (H3Y-K14Q = hht2(K14Q, L109I, A110W, L130I), HHF2, LEU2)	PKY4701	This study (Fig. 3)
PKY4779 (K14R wt-c)	+ p104 (H3-K14R = hht2(K14R), HHF2, TRP1) +pRS415	PKY4701	This study (Fig. 3-S2)
PKY4781 (K14R mXY)	+P105 (H3X-K14R = hht2(K14R, L126A, L130V), HHF2, TRP1) + pH3Y (H3Y = hht2(L109I, A110W, L130I), HHF2, LEU2)	PKY4701	This study (Fig. 3)
PKY4783 (K14R XmY)	+ pH3X (H3X = hht2(L126A, L130V), HHF2, TRP1) +P106 (H3Y-K14R = hht2(K14R, L109I, A110W, L130I), HHF2, LEU2)	PKY4701	This study (Fig. 3)
PKY4786 (K14R mXmY)	+P105 (H3X-K14R = hht2(K14R, L126A, L130V), HHF2, TRP1) +P106 (H3Y-K14R = hht2(K14R, L109I, A110W, L130I), HHF2, LEU2)	PKY4701	This study (Fig. 3)
PKY4805 (K18Q mXY)	+P114 (H3X-K18Q = hht2(K18Q, L126A, L130V), HHF2, TRP1) + pH3Y (H3Y = hht2(L109I, A110W, L130I), HHF2, LEU2)	PKY4701	This study (Fig. 3)
PKY4807 (K18Q XmY)	+ pH3X (H3X = hht2(L126A, L130V), HHF2, TRP1) +P115 (H3Y-K18Q = hht2(K18Q, L109I, A110W, L130I), HHF2, LEU2)	PKY4701	This study (Fig. 3)

PKY4809 (K18Q mXmY)	+P114 (H3X-K18Q = hht2(K18Q, L126A, L130V), HHF2, TRP1) +P115 (H3Y-K18Q = hht2(K18Q, L109I, A110W, L130I), HHF2, LEU2)	PKY4701	This study (Fig. 3)
PKY4797 (K18R mXY)	+P111 (H3X-K18R = hht2(K18R, L126A, L130V), HHF2, TRP1) + pH3Y (H3Y = hht2(L109I, A110W, L130I), HHF2, LEU2)	PKY4701	This study (Fig. 3)
PKY4799 (K18R XmY)	+ pH3X (H3X = hht2(L126A, L130V), HHF2, TRP1) +P112 (H3Y-K18R = hht2(K18R, L109I, A110W, L130I), HHF2, LEU2)	PKY4701	This study (Fig. 3)
PKY4801 (K18R mXmY)	+P111 (H3X-K18R = hht2(K18R, L126A, L130V), HHF2, TRP1) +P112 (H3Y-K18R = hht2(K18R, L109I, A110W, L130I), HHF2, LEU2)	PKY4701	This study (Fig. 3)
PKY4822 (K27Q mXY)	+P120 (H3X-K27Q = hht2(K27Q, L126A, L130V), HHF2, TRP1) + pH3Y (H3Y = hht2(L109I, A110W, L130I), HHF2, LEU2)	PKY4701	This study (Fig. 3)
PKY4823 (K27Q XmY)	+ pH3X (H3X = hht2(L126A, L130V), HHF2, TRP1) +P121 (H3Y-K27Q = hht2(K27Q, L109I, A110W, L130I), HHF2, LEU2)	PKY4701	This study (Fig. 3)
PKY4825 (K27Q mXmY)	+P120 (H3X-K27Q = hht2(K27Q, L126A, L130V), HHF2, TRP1) +P121 (H3Y-K27Q = hht2(K27Q, L109I, A110W, L130I), HHF2, LEU2)	PKY4701	This study (Fig. 3)
PKY4813 (K27R mXY)	+P127 (H3X-K27R = hht2(K27R, L126A, L130V), HHF2, TRP1) + pH3Y (H3Y = hht2(L109I, A110W, L130I), HHF2, LEU2)	PKY4701	This study (Fig. 3)
PKY4815 (K27R XmY)	+ pH3X (H3X = hht2(L126A, L130V), HHF2, TRP1) +P128 (H3Y-K27R = hht2(K27R, L109I, A110W, L130I), HHF2, LEU2)	PKY4701	This study (Fig. 3)
PKY4817 (K27R mXmY)	+P127 (H3X-K27R = hht2(K27R, L126A, L130V), HHF2, TRP1) +P128 (H3Y-K27R = hht2(K27R, L109I, A110W, L130I), HHF2, LEU2)	PKY4701	This study (Fig. 3)
PKY4827 (K36Q wt-c)	+ p122 (H3-K36Q = hht2(K36Q), HHF2, TRP1) +pRS415	PKY4701	This study (Fig. 3-S2, 4)
PKY4829 (K36Q mXY)	+P123 (H3X-K36Q = hht2(K36Q, L126A, L130V), HHF2, TRP1) + pH3Y (H3Y = hht2(L109I, A110W, L130I), HHF2, LEU2)	PKY4701	This study (Fig. 3, 4)
PKY4831 (K36Q XmY)	+ pH3X (H3X = hht2(L126A, L130V), HHF2, TRP1) +P124 (H3Y-K36Q = hht2(K36Q, L109I, A110W, L130I), HHF2, LEU2)	PKY4701	This study (Fig. 3, 4)
PKY4834 (K36Q mXmY)	+P123 (H3X-K36Q = hht2(K36Q, L126A, L130V), HHF2, TRP1) +P124 (H3Y-K36Q = hht2(K36Q, L109I, A110W, L130I), HHF2, LEU2)	PKY4701	This study (Fig. 3, 4)
PKY4837 (K37Q mXY)	+P126 (H3X-K37Q = hht2(K37Q, L126A, L130V), HHF2, TRP1) + pH3Y (H3Y = hht2(L109I, A110W, L130I), HHF2, LEU2)	PKY4701	This study (Fig. 3)
PKY4839 (K37Q XmY)	+ pH3X (H3X = hht2(L126A, L130V), HHF2, TRP1) +P127 (H3Y-K37Q = hht2(K37Q, L109I, A110W, L130I), HHF2, LEU2)	PKY4701	This study (Fig. 3, 4)

PKY4841 (K37Q mXmY)	+P126 (H3X-K37Q = hht2(K37Q, L126A, L130V), HHF2, TRP1) +P127 (H3Y-K37Q = hht2(K37Q, L109I, A110W, L130I), HHF2, LEU2)	PKY4701	This study (Fig. 3, 4)
PKY5031 (P38V wt-c)	+ p160 (H3-P38V = hht2(P38V), HHF2, TRP1) +pRS415	PKY4701	This study (Fig. 3-S2, 4)
PKY5033 (P38V mXY)	+P161 (H3X-P38V = hht2(P38V, L126A, L130V), HHF2, TRP1) + pH3Y (H3Y = hht2(L109I, A110W, L130I), HHF2, LEU2)	PKY4701	This study (Fig. 3, 4)
PKY5035 (P38V XmY)	+ pH3X (H3X = hht2(L126A, L130V), HHF2, TRP1) +P162 (H3Y- P38V = hht2(P38V, L109I, A110W, L130I), HHF2, LEU2)	PKY4701	This study (Fig. 3, 4)
PKY5037 (P38V mXmY)	+P161 (H3X-P38V = hht2(P38V, L126A, L130V), HHF2, TRP1) +P162 (H3Y- P38V = hht2(P38V, L109I, A110W, L130I), HHF2, LEU2)	PKY4701	This study (Fig. 3, 4)
PKY5138 (K36Q_X/P38V_Y)	+P123 (H3X-K36Q = hht2(K36Q, L126A, L130V), HHF2, TRP1) +P162 (H3Y- P38V = hht2(P38V, L109I, A110W, L130I), HHF2, LEU2)	PKY4701	This study (Fig. 3)
PKY5140 (P38V_X/K36Q_Y)	+P161 (H3X-P38V = hht2(P38V, L126A, L130V), HHF2, TRP1) +P124 (H3Y-K36Q = hht2(K36Q, L109I, A110W, L130I), HHF2, LEU2)	PKY4701	This study (Fig. 3)
PKY4843 (K56R wt-c)	+ p128 (H3-K56R = hht2(K56R), HHF2, TRP1) +pRS415	PKY4701	This study (Fig. 3-S2)
PKY5077 (*eaf3Δ* WT wt-c)	MAT**a**; Δ(*hht-hhf1*); Δ(*hht2-hhf2*); *leu2-3,112*; *ura3-62*; *trp1*; *his3*; *eaf3::KanMX4* + pPK188 (HHT2-HHF2, URA3, CEN), isolate 1	PKY4701	This study (Fig. 4)
PKY5078 (*eaf3Δ* WT wt-c)	MAT**a**; Δ(*hht-hhf1*); Δ(*hht2-hhf2*); *leu2-3,112*; *ura3-62*; *trp1*; *his3*; *eaf3::KanMX4* + pPK188 (HHT2-HHF2, URA3, CEN), isolate 2	PKY4701	This study
PKY5081 (*eaf3Δ* pWT XY)	+pH3X (H3X = hht2(L126A, L130V), HHF2, TRP1) +pH3Y (H3Y = hht2(L109I, A110W, L130I), HHF2, LEU2)	PKY5077	This study (Fig. 4)
PKY5079 (*eaf3Δ* K36Q wt-c)	+ p122 (H3-K36Q = hht2(K36Q), HHF2, TRP1) +pRS415	PKY5077	This study (Fig. 4)
PKY5083 (*eaf3Δ* K36Q mXY)	+P123 (H3X-K36Q = hht2(K36Q, L126A, L130V), HHF2, TRP1) + pH3Y (H3Y = hht2(L109I, A110W, L130I), HHF2, LEU2)	PKY5077	This study (Fig. 4)
PKY5086 (*eaf3Δ* K36Q XmY)	+ pH3X (H3X = hht2(L126A, L130V), HHF2, TRP1) +P124 (H3Y-K36Q = hht2(K36Q, L109I, A110W, L130I), HHF2, LEU2)	PKY5078	This study (Fig. 4)
PKY5087 (*eaf3Δ* K36Q mXmY)	+P123 (H3X-K36Q = hht2(K36Q, L126A, L130V), HHF2, TRP1) +P124 (H3Y-K36Q = hht2(K36Q, L109I, A110W, L130I), HHF2, LEU2)	PKY5077	This study (Fig. 4)
PKY4574	+P65 (*BirA::HIS3* integration plasmid)	PKY4171	This study

PKY4610 (WT wt-C)	+ P66 (bio-H3 = biotin-hht2, HHF2, TRP1)	PKY4574	This study (Fig. 5)
PKY4983 (pWT-XY)	+P67 (bio-H3X = bio-hht2(L126A, L130V), HHF2, TRP1) + pH3Y (H3Y = hht2(L109I, A110W, L130I), HHF2, LEU2)	PKY4574	This study (Fig. 5)
PKY5003 (S10A wt-C)	+ P165 (bio-H3-S10A= biotin-hht2(S10A), HHF2, TRP1) +pRS415	PKY4574	This study (Fig. 5)
PKY5005 (S10A XY cis)	+P166 (bio-H3X-S10A = bio-hht2(S10A, L126A, L130V), HHF2, TRP1) + pH3Y (H3Y = hht2(L109I, A110W, L130I), HHF2, LEU2)	PKY4574	This study (Fig. 5)
PKY4986 (S10A XY trans)	+P67 (bio-H3X = bio-hht2(L126A, L130V), HHF2, TRP1) + p85 (H3Y-S10A = hht2(S10A, L109I, A110W, L130I), HHF2, LEU2)	PKY4574	This study (Fig. 5)
PKY5042 (S10A XY double)	+P166 (bio-H3X-S10A = bio-hht2(S10A, L126A, L130V), HHF2, TRP1) + p85 (H3Y-S10A = hht2(S10A, L109I, A110W, L130I), HHF2, LEU2)	PKY4574	This study (Fig. 5)